JOURNAL OF MATERIALS SCIENCE 24 (1989) 3956–3975

Microdamage analysis of fibrous composite monolayers under tensile stress

H. D. WAGNER†, L. W. STEENBAKKERS*
Polymeric Composites Laboratory, Department of Materials Research, The Weizmann Institute of Science, Rehovot 76100, Israel

The quasi-static deformation and fracture modes of several types of fibrous composite materials are studied from a fundamental viewpoint using a new experimental approach. Microcomposite monolayers, consisting of single fibres accurately positioned into a thin polymeric matrix, were manufactured using a specially developed technique, and tested for strength by means of a custom-made miniature tensile testing machine. The materials used were E-glass, and Kevlar 29, Kevlar 49 and Kevlar 149 para-aramid fibres, and a room-temperature curing epoxy resin. The tensile testing machine was fitted to the stage of a polarized light stereozoom microscope and the fracture process was recorded both via a standard 35 mm camera and a colour video camera. The fibre content of the first generation of microcomposite monolayers used in this work was low (<0.025) but definite effects on the modulus and strength were obtained as the experimental data followed the rule-of-mixtures quite accurately in most cases. The failure process was different in each type of composite and current statistical models for strength are unable to account for the modes of failure observed in some of the systems studied. The experimental approach proposed is potentially useful in the study of the effects of interface chemistry modifications, fibre–fibre interactions, matrix toughness modification, misalignment effects, and more, on the deformation and failure micromechanics of composites.

1. Introduction

The fracture behaviour of fibrous composites is characterized by the combination of complex microdamage events such as fibre breakage, interface decohesion, matrix failure, to mention a few. An important material characteristic contributing to the complexity of the failure process in composite structure is the failure mode of each of the composite constituents, which depends strongly on the material microstructure, including its degree of homogeneity and anisotropy. Other key contributing factors are the type of applied loading, the internal geometrical features of the composite, the nature of the fibre–matrix interface, and the fibre content. As a direct consequence of the complexity of the damage encountered in "real-life" composites, only simple geometrical and loading cases may at first be studied, if the basic mechanical behaviour and damage modes are to be understood from a fundamental viewpoint.

The simplest geometry for a fibrous composite solid is a monolayer tape made of parallel and continuous fibres embedded in a matrix, as shown schematically in Fig. 1. In the past, various theoretical and experimental studies focused upon this idealized view of a composite to examine its behaviour under axial tensile stress. Based on actual material behaviour, in most of these studies the mean failure strain of the fibres was assumed to be lower than the mean failure strain of the matrix, which has the consequence – at least in an idealized context – that fibre breakage is viewed as the triggering event in the tensile failure process, the matrix playing a secondary, "passive", role. Moreover, for mathematical convenience and simplicity, the interface was often assumed to be infinitely strong. It has also been assumed, and verified experimentally in most cases, that the fibre strength is not a deterministic variable but, rather, is essentially a statistical parameter. An important consequence of these key assumptions is that the mechanical breakdown phenomenon in these materials is a complicated stochastic process involving scattered fibre breaking at weaker sites, which reflects the inherent statistical variability in fibre strength, and local overloading and failure of neighbouring fibres by way of stress transfer through the matrix. Final failure of the composite results through the rapid growth of a cluster of adjacent fibre breaks possessing a critical dimension. Obviously if the fibre strength was not a random variable, failure of a fibre would result in the immediate failure of all adjacent fibres (assumed to be of the same type), because the load transferred from the broken fibre to its neighbours would immediately increase the stress in these latter above their (deterministic) strength.

Most recently, microcomposite monolayers

*Present address: DSM Research, Geleen, The Netherlands.
†Incumbent of the Jacob and Alphonse Laniado Career Development Chair.

0022–2461/89 $03.00 + .12

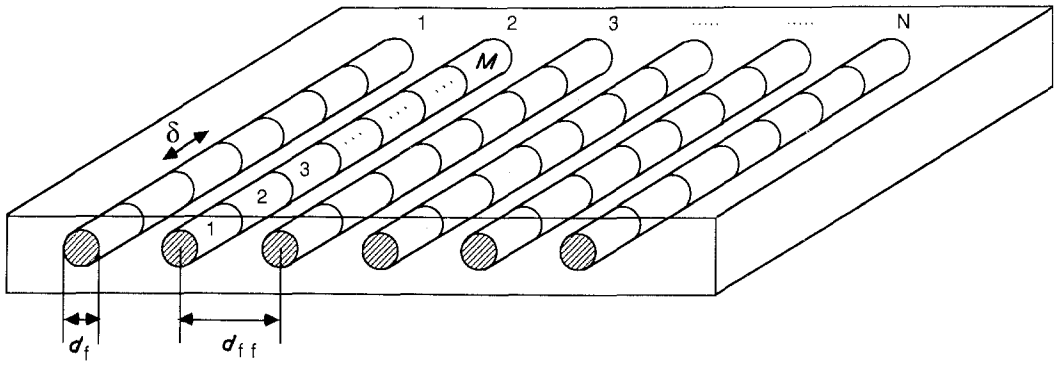

Figure 1 Schematic representation of microcomposite monolayer consisting of N parallel single filaments embedded in a thin polymeric matrix film. This structure is partitioned into M longitudinal elements of length δ. The fibre diameter is d_f and the interfibre distance is d_{ff}.

containing tape-like arrays of carefully positioned single aramid fibres within an epoxy resin have been successfully prepared and tested for strength by Wagner [1] and Steenbakkers and Wagner [2]. (See also [3] on related work.) In the present work, an experimental study of the elastic properties and mechanical damage behaviour of several types of microcomposite monolayers, including hybrids, is carried out. The effect of fibre type and fibre content on the elastic and fracture properties of the microcomposites is examined. The potential usefulness of such microcomposite monolayers in the characterization of basic failure modes of fibre-reinforced composites, and of the dynamics of failure in such materials, is demonstrated by means of video microphotography. The video microphotographic observation of the failure process in composite materials is used also as a probing tool for some of the basic hypotheses in current probabilistic theories of composite strength. Various areas of future research using the experimental approach taken in the present study are suggested.

2. General features of the failure process in composites

The tensile failure of assemblies of fibres, such as yarns and unidirectional composites, is a complex statistical phenomenon involving several modes of failure arising simultaneously. Daniels [4], Coleman [5], Gucer and Gurland [6], and Scop and Argon [7] were among the first to analyse in detail the failure mechanics of bundles of parallel fibres and composite monolayers from a probabilistic viewpoint. In the simplest case equal sharing among all fibres in a cross-section of the load released by a broken fibre was assumed. Rosen [8] performed the first experiments on such tape-like structures using glass/epoxy composites, but predicted theoretically that the composite strength should be independent of size, in contradiction with experimental results. Later, Zweben [9], Scop and Argon [10], Zweben and Rosen [11], Argon [12], produced new results for the case of local sharing of the load among the immediate neighbours of a broken fibre, a situation which is more appropriate for composite materials. Several forms of local load-sharing rules are reviewed and discussed in Smith *et al.* [13].

Key features for the strength of composites can be summarised as follows.

(a) The Weibull distribution [14] is generally observed to fit satisfactorily experimental results for the strength of single fibres of equal shape and size (for the strength and lifetime distributions of para-aramid fibres see [15, 16]). This failure probability distribution, originally introduced from an empirical viewpoint, is given as

$$F(x) = 1 - \exp\left[-l\left(\frac{x}{a}\right)^b\right] \qquad x \geqslant 0 \quad (1)$$

where $F(x)$ is the probability of failure of a fibre of length l under an applied stress less than or equal to x, a is the scale parameter and b is the shape parameter. Various versions and modifications of Equation 1 were recently proposed to include the effects of length and diameter variability [1, 17–19]. This function is currently the most popular scheme in use for describing the ultimate mechanical behaviour of solids having a linear stress–strain behaviour up to breakdown. It has been used to describe extreme-value problems as varied as the propagation of cracks along a geological fault, the collapse of fractal trees, the failure of vacuum-tubes, the analysis of carcinogenesis test results, and more (see Wagner [19] and references therein). The Weibull distribution has been recently justified from a microscopic viewpoint via mechanistic [20, 21], kinetic [22, 23], and percolation-based arguments [24]. The Weibull distribution for single-fibre strength may be determined from tests on the single fibres but there is a certain degree of uncertainty regarding the applicability of results on single fibres tested outside the composite matrix to the behaviour of the fibres within the matrix. To date there is no simple solution to this problem.

(b) Simple models of the failure process (see Appendix) consider that as a group of k adjacent broken fibres reaches a critical value, say k^*, the stress concentration factors become so large that the composite fails catastrophically. The value of k^* is generally assumed to vary between 3 and 8, depending on the system, and although some experimental work on this has been performed, there is no definite evidence for the value of k^* for a given composite system, and no study was made of the possible dependence of k^* on the interfibre distance, composite thickness and other variables. The value of k^* may be predicted (see Equation 41 in Phoenix [25]) based on various materials parameters. The computation of the stress concentration factors is a difficult task which was initiated by Hedgepeth [26], Hedgepeth and Van Dyke [27] and Fichter [28]. Detailed probabilistic analyses

were developed by Harlow and Phoenix [29, 30] and more recent work on this was performed by Smith *et al.* [13], Fukuda and Kawata [31], Reedy [32], Batdorf and Ko [33], Bader and Pitkethly [34], and Wolstenholme and Smith [35].

(c) Along a fibre length, the stress concentration arising from a broken site on that fibre is restricted to a relatively short length δ, assumed by most researchers to be of the order of ten fibre diameters (however, Fukuda and Kawata [31] suggest a much larger value if the matrix bears tensile stress as well). This length is the ineffective length (Rosen [8]), also termed the stress-transfer or interaction length. Across the composite width, some form of local load sharing is certainly a better approximation to experimental reality than equal load sharing.

(d) From the models in (b) and (c) above, and as shown in the Appendix, assuming that the single-fibre distribution is of the Weibull type, a Weibull distribution results for the composite strength (but again with the problem mentioned before that the strength distribution of single fibres inside a matrix may not necessarily be identical to the distribution of fibres outside it). The parameters of the Weibull distributions of the composite and the fibre are formally related, the relation being particularly simple for the shape parameters where the ratio of composite to single-fibre parameters is exactly equal to k^* (Equation A3). The relation for the scale parameters (Equation A4) is more complex and involves various materials and mechanical constants, including the stress concentration factors, the number of nearest neighbours adjacent to a fibre break, the transfer length, and the shape and scale parameters of the single fibre.

Experimental work aimed at understanding the critical failure modes in simple composites containing idealized fibre arrays, such as Rosen's work on tape-like structures [8], is relatively scarce, and is currently the subject of renewed interest. Early photoelastic studies of the stress field in the vicinity of fibre discontinuities were performed by Schuster and Scala [36], Tyson and Davies [37], Pih and Sutliff [38], MacLaughlin [39] and others, using mainly experimental models of composites. Probably the most informative early studies on failure mechanisms were those of Rosen [8] who used high-speed photography with thick glass fibre in epoxy resin, McKee and Sines [40] who proposed an alternative statistical model for strength including the effect of size, Friedman [41] who generalized Rosen's theory to deal with fibres with variable diameter and length and performed experiments with glass and boron composites, Armenakas *et al.* [42] who established the strength characteristics of S-glass fibre bundles and composites using interference Moiré methods, and Mullin *et al.* [43] who examined the fracture modes of single and multiple filaments of boron in epoxy resin. Recent work on the determination of the critical transfer (or interaction) length, using fragmentation of a single fibre in a ductile matrix, includes the studies of Fraser *et al.* [44], Drzal *et al.* [45], Jacques and Favre [46], Bascom *et al.* [47], Piggott *et al.* [48], and DiLandro *et al.* [49].

The understanding of fundamental failure modes in unidirectional composites is still far from being achieved and, as stated before, is currently the subject of renewed interest. Recent work includes Watson and Smith [18] and Bader and Pitkethly [34] who studied the failure of hybrids using probability concepts, and Wolstenholme and Smith [35] who attempted to assess the effect of varying inter-tow distance on the stress concentration factors and the critical (stress transfer) length. It is now well accepted that probabilistic modelling is a necessary tool for a satisfactory understanding of composite failure, and the aim of most recent experimental studies was to assess the values of various parameters included in the theoretical models as well as to verify the validity of such models.

With the above motivations, an experimental programme was initiated in our laboratory with the aim of understanding basic deformation and failure modes in several types of model composite materials, including those composites which fail by a mode not in accordance with some of the basic hypotheses of current statistical approaches to failure (these hypotheses are listed in the Appendix). The specific goals of our research are: (a) to manufacture accurate single-fibre microcomposite monolayers; (b) to perform careful mechanical testing; (c) to monitor the failure process by means of video microphotography. In the present paper we report first results along these lines, using the first generation of microcomposite monolayers produced in our laboratory.

3. Experimental procedure

3.1. Materials

The matrix used in the present study was a room-temperature curing, low viscosity, bisphenol A-based epoxy resin, modified with cresyl glycidal ether, (Araldite CY 223 from Ciba Geigy) mixed with a polyamine hardener (HY 956 from Ciba Geigy) in the proportions suggested by the manufacturer. The cure schedule was 7 d at 25° C.

The fibres used were (a) para-aramid poly-*p*-phenylene terephthalamides (Kevlar 29, Kevlar 49 and Kevlar 149) produced by du Pont de Nemours and Co. Inc., Wilmington, Delaware, extracted from spools containing 267 fibres per yarn for Kevlar 29 and Kevlar 49, and 768 fibres per yarn for Kevlar 149; (b) E-glass (EC-R099-320) produced by Vetrotex Ltd., extracted from spools containing 816 fibres per yarn. Kevlar 29 and Kevlar 49 have similar high strength but the latter has twice the elastic modulus of the former. The properties of the more recent Kevlar 149 fibre have been studied recently in our laboratory [50, 51]. Some information on Kevlar 149 fibres is also available from the study of Riewald *et al.* [52]. According to this study, Kevlar 149 has a strain to failure of about 1.5 percent, a modulus of about 150-160 GPa, and a tensile strength of about 2.4 GPa, but we found these latter two properties to be highly dependent on the fibre diameter and length [50, 51]. As compared to previous versions of Kevlar, Kevlar 149 has a much lower moisture pickup tendency, and a slightly higher density. All fibres in the present study were utilized in their as-received condition, and no attempt was made either to remove or modify any surface sizing treatment.

3.2. Manufacture of epoxy films and microcomposite monolayers

3.2.1. Manufacture of epoxy films

Commercially available 7 × 7 cm^2 transparent PVC plates, with a thin layer of silicone oil deposited on them, were used for moulding epoxy films. The silicone oil layer was used to prevent the cured epoxy film from sticking to the PVC plates. Double-sided 50 μm thick adhesive tape, used as spacer, was positioned on two opposite edges of one PVC plate, and freshly prepared epoxy resin was carefully poured between the spacers. Subsequently, the second PVC plate was put on top of the first one, and after air bubbles were expressed, a 5 kPa pressure was applied to the mould. The epoxy was cured at room temperature (24 ± 2° C) for at least 2 d before the two plates were separated, and then left to cure for another 5 d before being cut to its final size using a specially designed cutter. Afterwards, the samples were tabbed on both sides with cardboard. The specimen width in its central part was 2 mm and its thickness varied (from specimen to specimen) between 40 and 100 μm.

3.2.2. Manufacture of microcomposites monolayers

Several samples containing one single fibre were prepared by glueing a fibre on both ends of a PVC plate using a fast setting cyanoacrylate adhesive. The rest of the manufacturing procedure was identical to that used for epoxy films, as described before. Microcomposite monolayers containing eight single fibres within epoxy were manufactured using the following two-stage procedure: (a) accurate positioning of the fibres so as to obtain a desired interfibre distance; (b) moulding of the fibre array into epoxy. This procedure is now described in detail.

3.2.2.1. Fibre positioning. To align the single fibres and control the distance between them, a single fibre positioner was specially designed and built in our laboratory. It consists of the following parts (refer to Fig. 2).

(i) Two rotation stages, on which the fibre guides are fastened. The stages are able to rotate the guides with an accuracy of 1/60°.

(ii) Two fibre guides, the most recent version of which consists of 20 thin cylindrical syringe rods, with a length of about 10 mm, and a diameter of 400 μm. The edge-to-edge distance between two syringe rods is 150 μm. When the rotation stage is straight (that is, when the aligned rods are perpendicular to the fibre longitudinal axis before rotation) the centre-to-centre distance between the single fibres is 550 μm. When the position of the guide is changed by rotating the positioner to an angle of θ (see Fig. 3), the centre-to-centre distance between the fibres is reduced to 550 cos (θ) μm. Because the diameter of the rods is much larger than the diameter of the fibres, the brittle and ductile fibres are forced to bend by virtually the same amount. In an early version of this single-fibre positioner, described in [1], parallel grooves were successfully used as fibre guides to bring the single fibres into position. This was a particularly convenient solution for microcomposites in which tough fibres like the aramids are used, but it was very difficult to bring brittle fibres such as E-glass in close vicinity due to the sharpness of the corners of the grooves which caused fibre breakage. Also differences in the flexural behaviour of different single fibres made it difficult to get an accurate control of the interfibre distance, especially when fibres of different diameters, or fibres of different types (in hybrids) are used. Thus, compared with the first version of the apparatus, in the current version the interfibre distance is much less affected by differences in bending behaviour, and brittle fibres can be mounted easily.

(iii) Two teflon rods, held horizontally on stands and containing slots for each fibre, are used to keep the fibres in position on the outside of the two guides.

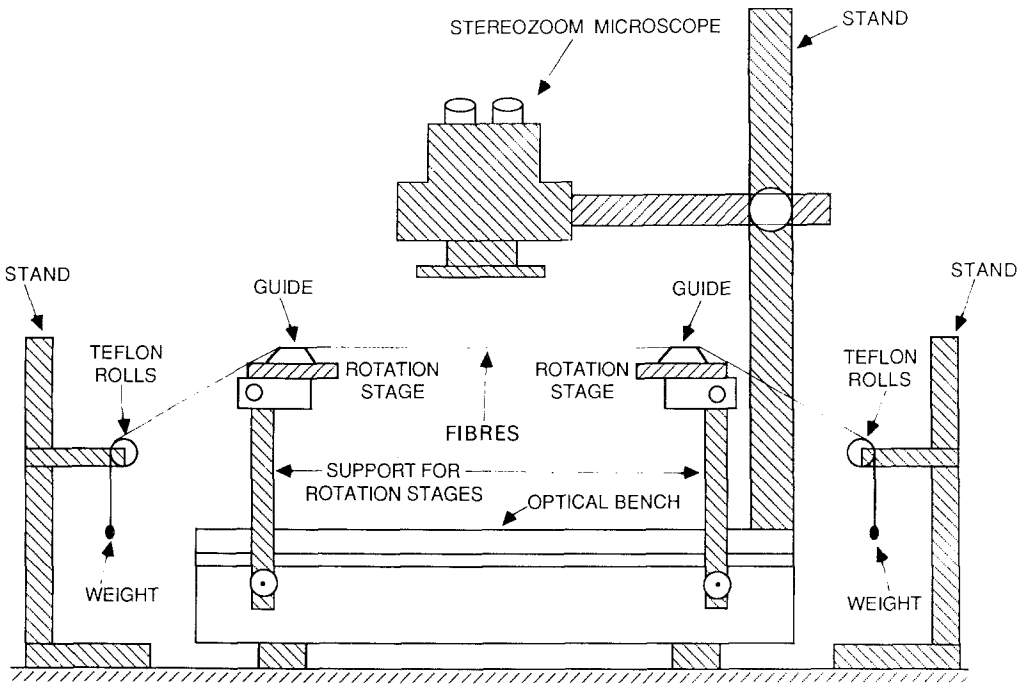

Figure 2 General view of the single-fibre positioner apparatus.

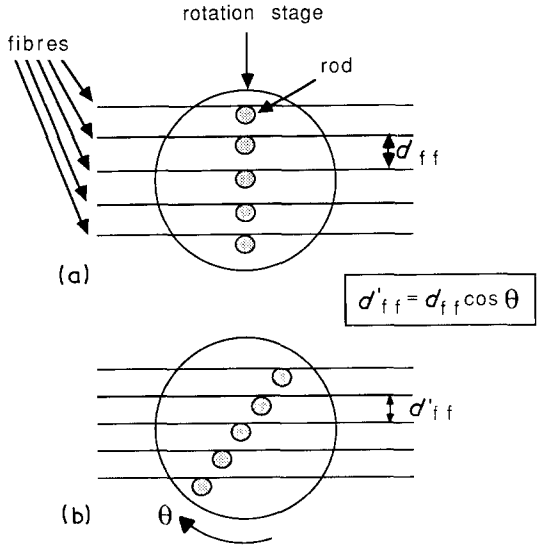

Figure 3 Illustration of the principle for varying the fibre-to-fibre distance: assuming an original interfibre spacing d_{ff}, a rotation θ of the fibre guides yields a new spacing $d'_{ff} = d_{ff} \cos \theta$.

(iv) Individual fibre weights of 0.75 g each were used to keep the single fibres under tension. These are lead fishing weights, tied to the ends of the single fibres. 0.75 g weights were normally used to hold the glass fibres and 1.50 g weights were used for the aramid fibres. (Notice that the fibres were selected so as to minimize diameter variability among themselves, thus eliminating the need for individualized weights in order to keep a constant tension stress in the fibres).

All parts of the positioner just described were mounted on an optical rail. The fibre mounting and alignment procedure was entirely performed with the help of a Stereozoom 7 (Bausch and Lomb) microscope.

3.2.2.2. Embedding the fibre array into epoxy. The second step in the manufacture of microcomposite monolayers consisted in embedding the fibre array into epoxy films, which was done as follows. After the fibres were brought into position and aligned according to the procedure outlined above, the interfibre distances were measured under the microscope as a check, and checked again after the moulding procedure was completed. The difficult of this step consisted mainly in leaving the fibre array undisturbed by the flowing epoxy during moulding. The fibre array was brought on to a PVC plate containing a thin layer of silicon oil, after a preliminary thin layer of the epoxy was poured on the plate between the two double-sided scotch tape spacers. (Without the preliminary layer, static electricity on the PVC plate would disturb the position of the fibres, but too thick a layer would also disturb the fibre array). The "wet" PVC plate was then placed on an optical table between the fibre guides (refer to Fig. 2) and lifted until it reached the fibre array. The fibres were then glued on both edges of the PVC plates using cyanoacrylate adhesive. About 5 min after this, when the adhesive was dry, freshly prepared epoxy was poured on top of the fibres (and of the first epoxy layer). A second PVC plate was then placed on top of the first plate, the air bubbles carefully expressed and a 5 kPa pressure applied on top of the upper plate. The mould was opened after 2 d and the samples were cut to size with the cutter used for epoxy samples.

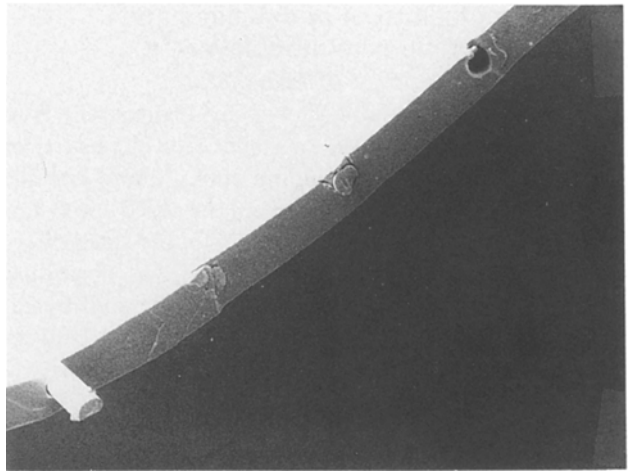

Figure 4 Scanning electron micrograph of an E-glass/epoxy microcomposite monolayer cross-section. Note the constant fibre-to-fibre distance and the planar arrangement of the fibres.

In the present study, all the microcomposite monolayers had a minimum edge-to-edge distance between the single filaments of about 40 μm with a variability of 7 to 15% depending on the interfibre distance and the type of fibre used. These figures are by no means limiting ones: much lower values of the fibre-to-fibre distance have already been obtained in our laboratory, and results using these will be reported in the near future. An example of a microcomposite monolayer sample is shown in Fig. 4. As seen, an accurate interfibre distance is obtained, and the fibres all lie within a plane. The thicker the monolayer, however, the closer the fibre plane lies close to one face, as will be seen later. This current limitation will hopefully be eliminated in the future.

3.3. Testing equipment and procedure

3.3.1. Testing equipment

A specially designed miniature tensile testing machine was built in our laboratory for the quasi-static tensile testing of the microcomposite monolayer specimens. This strain-controlled device was fitted to the stage of a polarized Zeiss microscope equipped with both a 35 mm camera and a Sony colour video camera for event recording during a test. The mini-tensile tester had a load cell of 20 kg, and the force was measured with an accuracy better than 3 g via a digital amplifier and an analogue recorder. A single-axis micropositioner (Oriel) was used for controlling the displacement of one of the clamps mounted on an optical table) with a repeatable accuracy of about 1 μm. Fig. 5 depicts the testing apparatus.

The single fibres were tested using a floor model Instron according to previously established tabbing, mounting, and testing procedures [15]. Epoxy films were also tested with the Instron machine for control purposes. Details of testing procedures are given in the following section.

3.3.2. Testing of single fibres and epoxy films

Young's modulus and the mechanical strength and strain of E-glass single fibres and epoxy films were

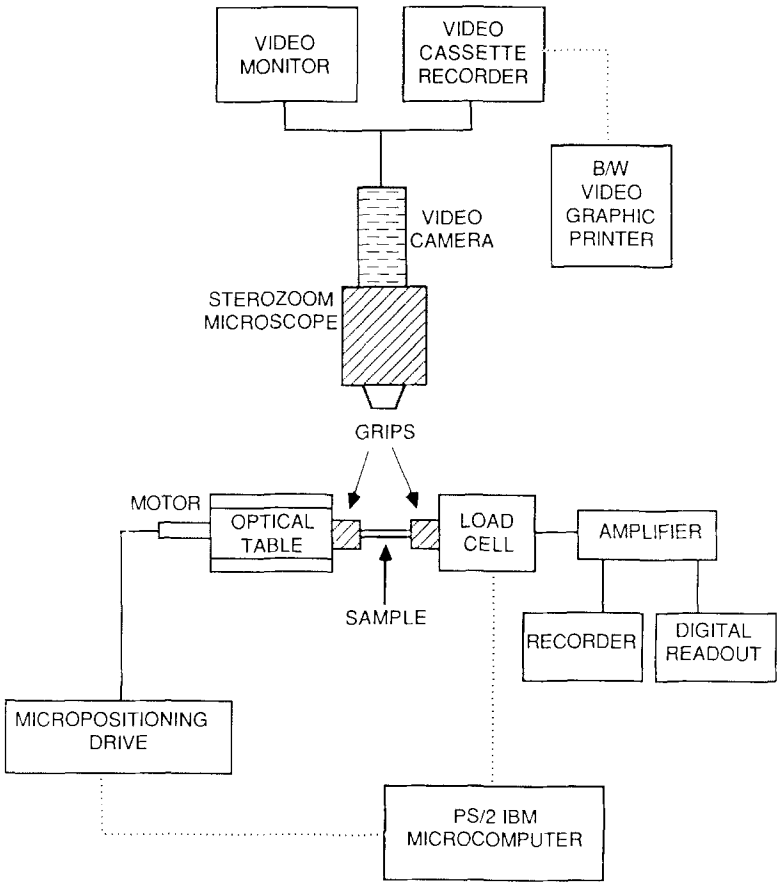

Figure 5 Schematic illustration of the experimental testing apparatus. As indicated, a black and white video graphic printer and a microcomputer are currently being added to the existing equipment.

determined by quasi-static tensile tests on the Instron machine using at least 30 samples in each case. An extension speed of 0.05 cm min^{-1} was used for E-glass fibres, and an extension speed of 0.3 cm min^{-1} was used for the epoxy samples. Additional tests were performed with epoxy samples using test conditions as for the microcomposites monolayers (see below). The gauge length used in these tests was 3 cm, and the epoxy films were clamped on both sides with cardboard using an epoxy glue. For E-glass fibres a cardboard frame was used, and just before testing the side strips of the frame were cut out [15]. The diameter of each single filament was measured several times at different positions along the length, by optical microscopy. The mechanical properties of the aramid single fibres were obtained from previous work [15, 50]. Results for the single fibres and the epoxy resin matrix are summarized in Table I.

3.3.3. Testing of microcomposite monolayers

All fibre diameters as well as fibre-to-fibre distances within a sample were measured before testing, and the means and coefficients of variation computed. The monolayer thickness was measured as well and its mean value calculated. From this the volume fraction of fibres was obtained for each specimen. The composites were checked to account for the presence of air bubbles and other visible damage, and seriously damaged samples were discarded. The microcomposites were tabbed in the same way as the epoxy films, by using cardboard tabs. The microcomposites were tested on the mini-tensile testing device at an extension speed

TABLE I Mechanical properties of single fibres and matrix used in this work. The data for Kevlar 29 and Kevlar 49 are taken from [2].

Material	Young's modulus, E (GPa) (c.v.)	Failure strain, ε (%) (c.v.)	Strength, σ (MPa) (c.v.)	n
Kevlar 29	58.9	4.0	2640	–
Kevlar 49	127.5	2.4	2640	–
Kevlar 149*	123.7	2.0	2640	50
	(0.16)	(0.14)	(0.21)	
E-Glass†	62.8	2.6	1540	30
	(0.08)	(0.26)	(0.25)	
CY223/HY956				
(1)‡	2.30	3.68	51	29
	(0.20)	(0.20)	(0.13)	
(2)§	1.98	3.01	37	18
	(0.22)	(0.23)	(0.15)	

*2 cm long samples, extension speed = 0.05 cm min^{-1}.
†3 cm long samples, extension speed = 0.05 cm min^{-1}.
‡Void-free epoxy samples with 3 cm gauge length, extension speed = 0.3 cm min^{-1}.
§Epoxy samples (occasionally with voids) with 2 cm gauge length, extension speed = 0.005 cm min^{-1}.

of 50 μm min^{-1}. The gauge length of the microcomposites was 2 cm, and testing was performed at room temperature. Particular care was taken to align accurately the microcomposites samples parallel to the testing axis of the tester. Evolution of the damage process was followed and recorded by video microphotography (Sony DXC-101 Single Chip CCD Colour Video Camera). Colour pictures with a standard 35 mm camera were taken as well. During loading, microdamage induced photoelastic patterns in the birefringent matrix, which provided a good indication of the extent of the microdamage region. After the tests were completed the fracture surface of a few selected samples was examined by scanning electron microscopy.

The mechanical properties which were measured include Young's modulus and the quasi-static strength and strain. Other interesting results, of a qualitative rather than of a quantitative nature, concern (a) the mode of failure of the various types of microcomposite monolayers, including the dynamics of the failure process which could be recorded by video microphotography, and (b) the assessment of the degree of accuracy of some of the hypotheses upon which current statistical theories of composite strength are based. The theories themselves cannot, however, be fully verified unless enough specimens are tested, which was not the purpose of the present work.

4. Results and discussion

4.1. Properties of single fibres and matrix

The Young's modulus, tensile strength and failure strain were measured for E-glass fibres, Kevlar 149 aramid fibres and CY223/HY956 epoxy films. Results are reported in Table I. The diameter of every fibre was measured at three sites along its length, and the thickness of the epoxy film was measured at five sites along its length, and the mean diameter value was calculated. No significant diameter variability was found along the length of the fibres, for all types, but significant diameter variability was found between the fibres, as observed previously [15]. A modified maximum likelihood estimation (MLE) procedure for the computation of Weibull scale and shape parameters was used to take diameter variability into account. Details of this statistical procedure are presented elsewhere [50, 51], jointly with modified Weibull plots for the case of Kevlar 149 fibres and a detailed study of size effects in this fibre. The properties of the Kevlar 29 and Kevlar 49 aramid fibres are also reported in Table I. It is seen that the Kevlar 49 and Kevlar 149 fibres tested in our laboratory have quite similar properties, except for the lower strain to failure of Kevlar 149. Note also the presence of helicoidally distributed flaws present in Kevlar 149 fibres [50].

The strain to failure of CY 223/HY 956 epoxy films varied between 0.030 and 0.037, depending on the amount of tiny air bubbles and other defects present.

4.2. Properties of microcomposite monolayers

A limited number of Kevlar 29/epoxy, Kevlar 49/epoxy, Kevlar 149/epoxy, E-glass/epoxy and hybrid Kevlar 29/Kevlar 149/epoxy microcomposite monolayers were tested using the mini-tensile testing device, as described previously. For each type, except the Kevlar 29/Kevlar 49/epoxy hybrid, both one- and eight-filament microcomposite monolayers were prepared and tested. One-filament microcomposites were tested to obtain indications of the behaviour of the filament when embedded in epoxy. Eight-filament microcomposites were tested to investigate possible fibre-to-fibre interactions which might take place during the failure process.

The mean edge-to-edge interfibre distance in the E-glass and Kevlar 49 microcomposites was 65 μm on average (with a coefficient of variation between 0.05 for the best sample and 0.14 for the worst sample). For Kevlar 29 and Kevlar 149 microcomposites this distance was 40 μm (with a coefficient of variation between 0.06 and 0.17). The thickness of the microcomposites was measured five times along the length, and the diameter of the fibre was determined using optical microscopy. In this way the fibre volume fraction, V_f, could be evaluated with maximum accuracy. The Young's modulus, strength, and failure strain were calculated and plotted as a function of fibre content for all types of microcomposites, including the baseline values for epoxy. The results in each specific case are now presented and discussed.

4.2.1. Kevlar 29/epoxy microcomposites

Eight microcomposites containing one Kevlar 29 filament and six microcomposites containing eight filaments were tested. The failure strain of the CY223/HY956 epoxy is slightly lower than that of the Kevlar 29 (Table I), thus the probability of having fibre breaks before matrix (or interface) failure is very low, as indeed is observed. In Figs 6a to c the Young's modulus, strength, and failure strain, respectively, are plotted against the volume fraction of fibres. Regarding the modulus, the Halpin–Tsai equation (or the rule-of-mixture, ROM) gives a good description of the measured data, as seen. For the strength, most experimental points are found under the ROM line, as is often observed in structural composites, but still the results show a definite increasing trend parallel to the ROM. For strain, again the results seem to follow a line parallel to the ROM.

Decohesion (or debonding) at the fibre/matrix interface is the major triggering fracture event in this system, as seen clearly from the video recordings. At debonding sites, conical cracks frequently appear in this system and grow through the matrix. From the video recordings it was noticed that as a side crack approaches the first fibre, the crack propagation speed decreases significantly (often reaching a near-zero value) probably because the presence of the fibre reduces the stress concentration factor ahead of the crack tip.

The sequence of photographs in Fig. 7 demonstrates typical failure processes in Kevlar 29/epoxy microcomposites comprising eight single filaments. In Fig. 7a the crack develops from a large matrix edge flaw, and as it approaches the first fibre the propagation speed decreases (as already noted above) and debonding of the first fibre occurs. This appears on the

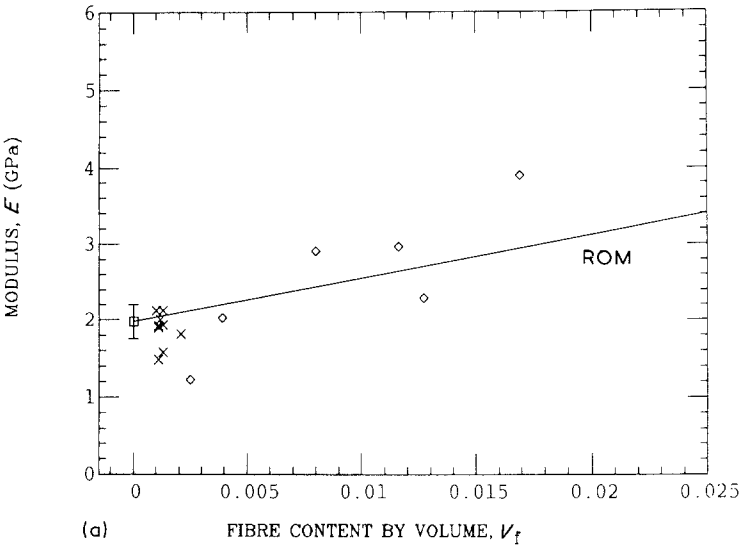

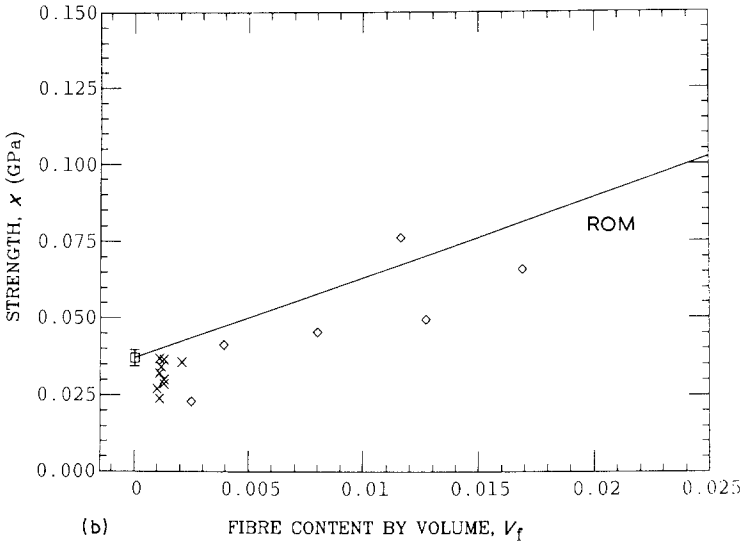

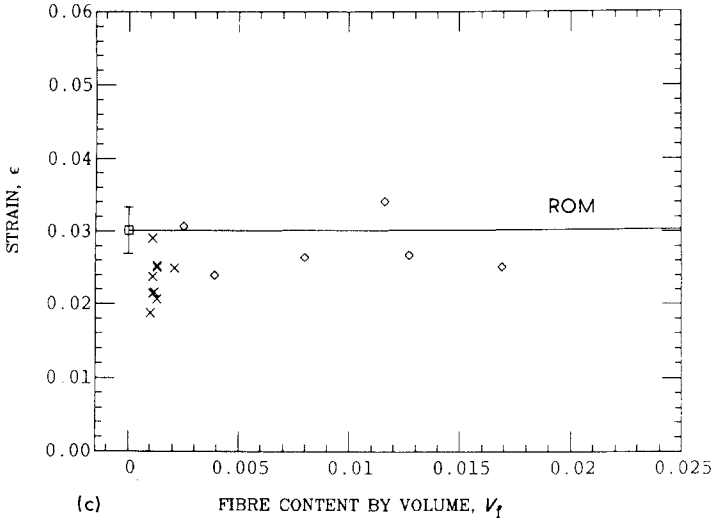

Figure 6 (a) Young's modulus, (b) tensile strength, (c) tensile strain at failure as a function of fibre content in Kevlar 29/epoxy microcomposite monolayers (Kevlar 29/CY223–HY956). (□) Epoxy film (95% c.i), (x) one-fibre monolayer, (◇) eight-fibre monolayer.

video recording as a dark zone around the fibre. After penetrating the fibre-rich zone via successive debonding events, the crack growth speed increases very rapidly as soon as the fourth fibre is reached, and catastrophic failure occurs. Thus, although debonding events rather than fibre break events are observed in this system, a "critical defect zone" as wide as four fibres is observed, which might perhaps be considered equivalent to the critical crack size, k^*, observed in composites in which fibre breaking is the main triggering event, and which are formally described by existing theoretical models (see Appendix).

Fig. 7b shows the failure process in a microcomposite containing no initial side crack in the matrix. Here the failure starts by fibre–matrix interface debonding (seen as a darker region) at several fibre sites, after which a matrix crack develops rapidly between the fibres, which fail by a progressive splitting mechanism.

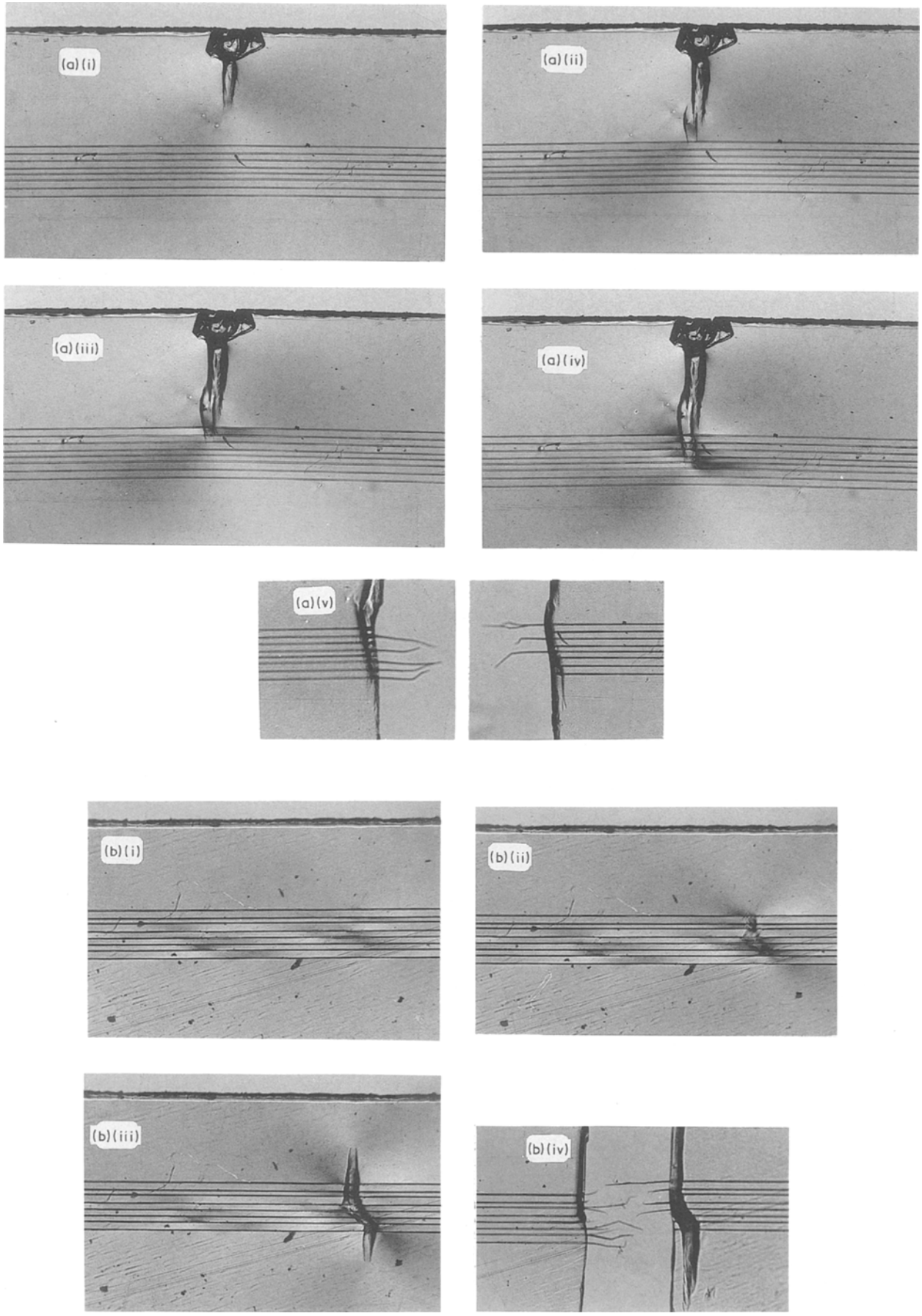

Figure 7 (a) Damage growth in Kevlar 29/epoxy microcomposite monolayer from an initial manufacturing defect in the matrix. (i) Relative stress RS (per cent of ultimate) = 0.91, number of debonded fibres $k = 0$; (ii) crack tip reaches first fibre, RS = 0.95, $k = 1$; (iii) slow crack growth by successive debonding of fibres, RS = 0.99, $k = 2$; (iv) fast (catastrophic) failure, RS = 0.97 (load has dropped), $k^* = 4$, debonded lengths are visible along each fibre; (v) broken halves of sample, showing pulled-out fibres of length equal to debonded length in (iv) above. (b) Damage growth in Kevlar 29/epoxy microcomposite monolayer from a defect within the fibre array. (i) Debonding (darker) zones appear as soon as relative applied stress RS is about 0.95; (ii) fast (catastrophic), failure at critical cluster, RS = 0.99, $k^* = 4$; (iii) RS = 0.97; (iv) broken halves of samples showing pulled-out fibres.

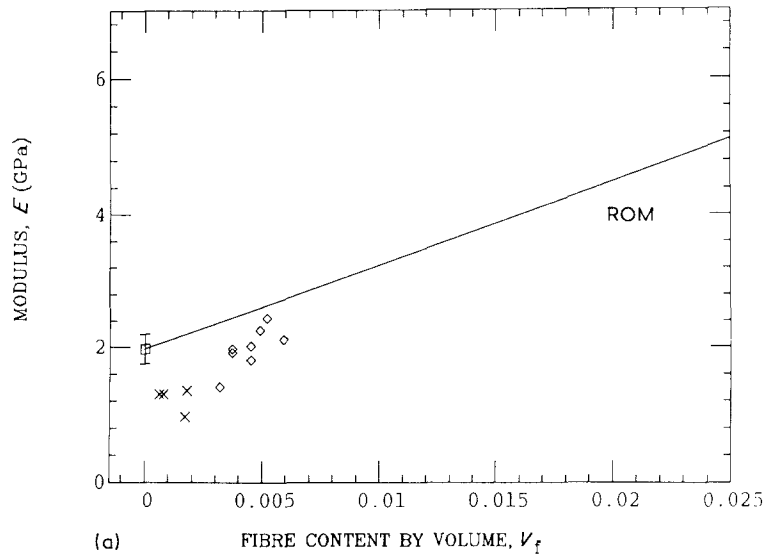

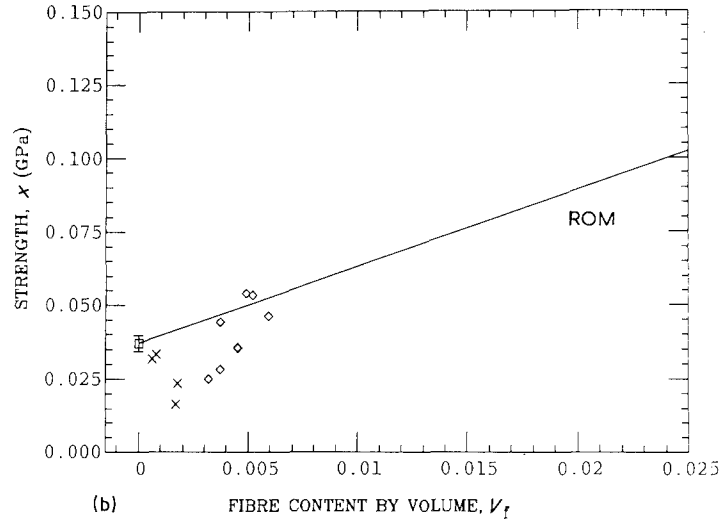

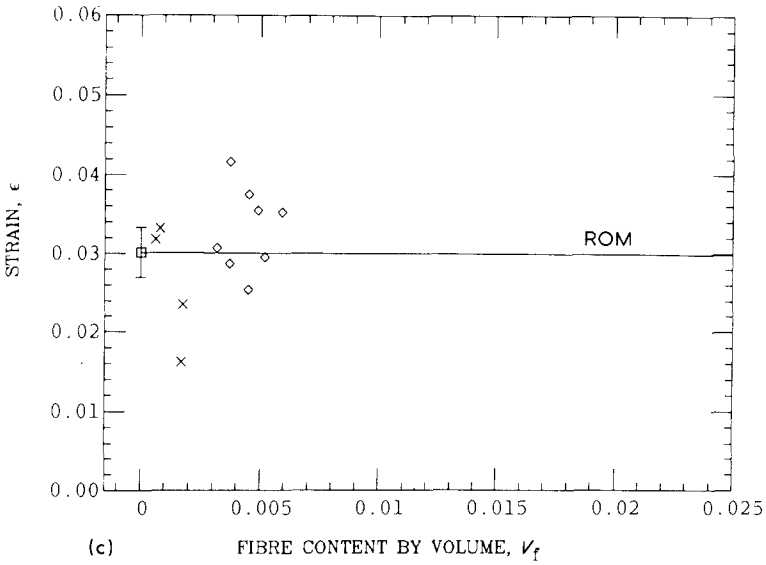

Figure 8 (a) Young's modulus, (b) tensile strength, (c) tensile strain at failure as a function of fibre content in Kevlar 49/epoxy microcomposite monolayers (Kevlar 49/CY223–HY956). (□) Epoxy film (95% c.i.), (x) one-fibre monolayer, (◇) eight-fibre monolayer.

4.2.2. Kevlar 49/epoxy microcomposites

Four microcomposites containing one Kevlar 49 filament and eight microcomposites containing eight filaments were tested. In this system the average strain to failure of the fibre is lower than the failure strain of the matrix (Table I), so in this case there is a higher probability of observing fibre breaks before the matrix starts failing. The experimental results for Young's modulus (Fig. 8a) follow approximately a monotonically increasing line, parallel to the ROM but the agreement is poorer than in the case of Kevlar 29/epoxy microcomposites. Also, the results for the pure epoxy are above most microcomposite data. Thus, the ROM line may be taken here as an upper bound for the modulus, and the observed deviations may possibly be due to a higher percentage of air bubbles. Nevertheless, the presence of fibres in the matrix has a definite positive effect on the modulus of the microcomposite.

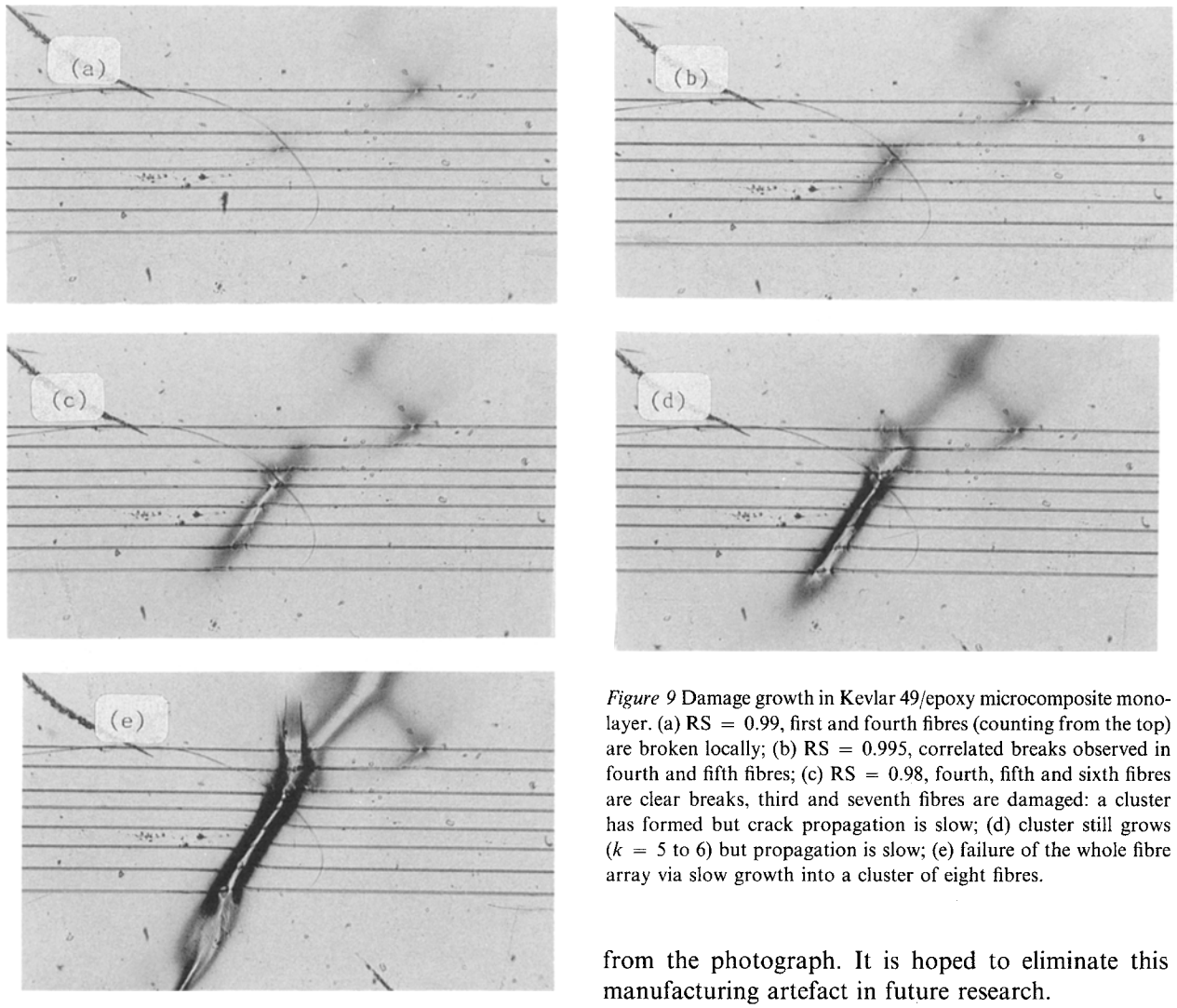

Figure 9 Damage growth in Kevlar 49/epoxy microcomposite monolayer. (a) RS = 0.99, first and fourth fibres (counting from the top) are broken locally; (b) RS = 0.995, correlated breaks observed in fourth and fifth fibres; (c) RS = 0.98, fourth, fifth and sixth fibres are clear breaks, third and seventh fibres are damaged: a cluster has formed but crack propagation is slow; (d) cluster still grows (k = 5 to 6) but propagation is slow; (e) failure of the whole fibre array via slow growth into a cluster of eight fibres.

The same observations and explanations as for the modulus are also appropriate for strength (Fig. 8b). As can be seen in Fig. 8c, the experimental data for the failure strain are more difficult to interpret in view of the large scatter.

Fig. 9 shows a series of photographs depicting the failure process in a Kevlar 49/epoxy microcomposite containing eight filaments. Here the major triggering event is fibre failure as expected. This is followed by the propagation of cracks into the matrix, causing more breaks in neighbouring fibres, until all fibres break in a progressive, slow, manner. Here, no critical crack size (at which catastrophic failure occurs) was observed, which can perhaps be explained by the large interfibre distance (about five fibre diameters). Another possibility is that the critical crack size is larger than 8 fibre breaks. Later we discuss the dynamics of failure in this system more in detail. From our observations, however, it was difficult to evaluate whether fibre–matrix bond failure also occurred or not. Fig. 10 is an SEM photograph of a Kevlar 49/epoxy microcomposite fracture surface, from which the quality of the specimen appears to be very satisfactory: the fibres lay in a single plane, and the interfibre distance is constant. However, as mentioned before, in thicker microcomposites the fibre plane lies closer to one side of the specimen, rater than in the midplane, as seen from the photograph. It is hoped to eliminate this manufacturing artefact in future research.

4.2.3. Kevlar 149/epoxy microcomposites

Five microcomposites containing one Kevlar 149 filament and 17 microcomposites containing eight filaments were tested. Again, as in the case of Kevlar 49/epoxy material, fibre break is likely to occur before any matrix failure event occurs, since the mean failure strain of the Kevlar 149 fibre is smaller than that of the epoxy matrix. Young's modulus, the strength and failure strain are plotted against the fibre content in Figs 11a to c, respectively. For the modulus and strength the experimental data are in very good agreement with the ROM line as seen for the Kevlar 29

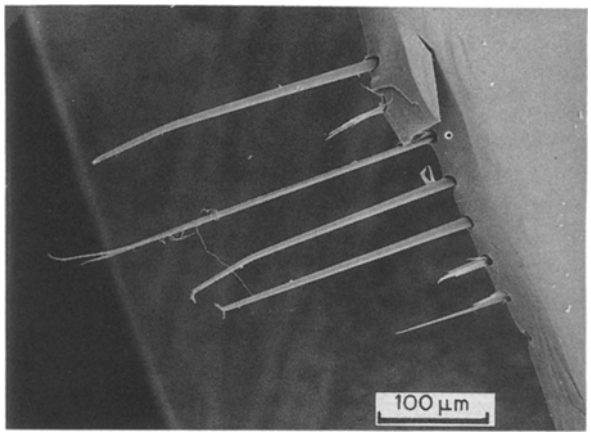

Figure 10 Scanning electron micrograph of a Kevlar 49/epoxy microcomposite monolayer after a fracture test.

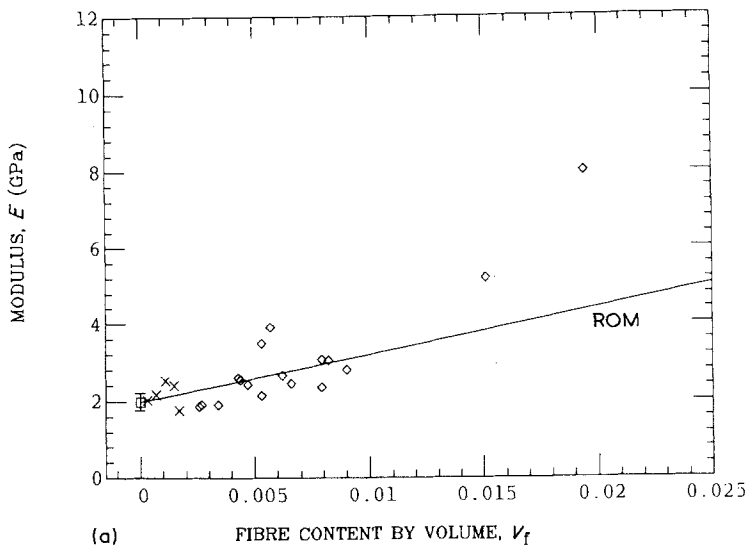

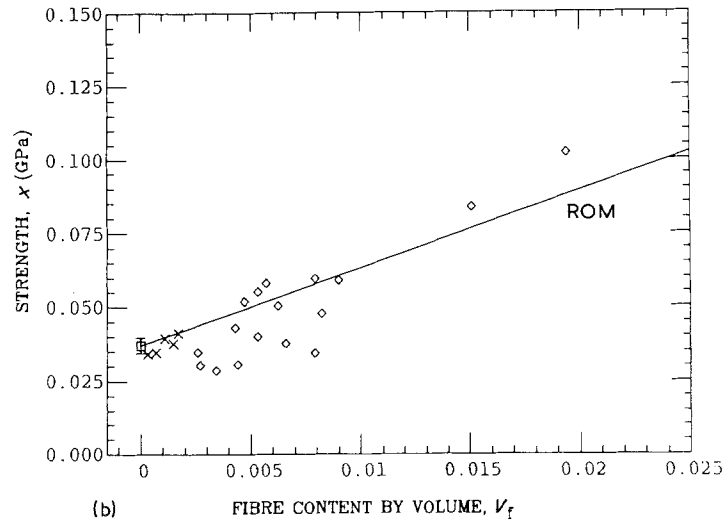

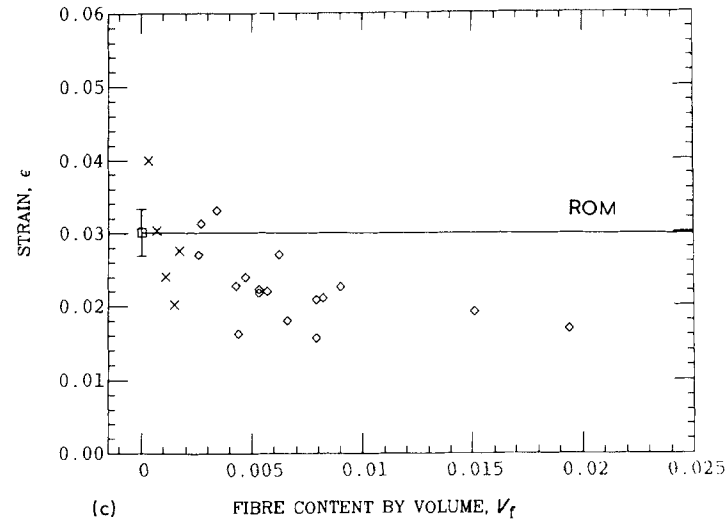

Figure 11 (a) Young's modulus, (b) tensile strength, (c) tensile strain at failure as a function of fibre content in Kevlar 149/epoxy microcomposite monolayers (Kevlar 149/CY223-HY956). (□) Epoxy film (95% c.i.), (x) one-fibre monolayer, (◇) eight-fibre monolayer.

microcomposites. The failure strain experimental line is seen to decrease faster than the ROM prediction, the reason for this trend being unclear at the present time.

Fibre fragmentation was observed to occur in a microcomposite containing one Kevlar 149 fibre (Fig. 12). This fragmentation process is similar to that occurring in carbon/epoxy single-fibre composites although (a) it is unclear whether or not saturation is attained in the present case because the difference in failure strains between the aramid and the epoxy is not very large, and (b) rather than being localized at single points along the fibre, the breaks are "delocalized", that is spread over a splitting length because aramid fibres do not break in a single fibre plane. In principle, the average fragment length can be used to calculate the critical length but the exact place of fibre break is difficult to determine because of fibre splitting. Nevertheless we are currently investigating the fragmentation process in low strain aramid fibres.

In Fig. 13 the damage growth process in a Kevlar 149/epoxy microcomposite containing eight single

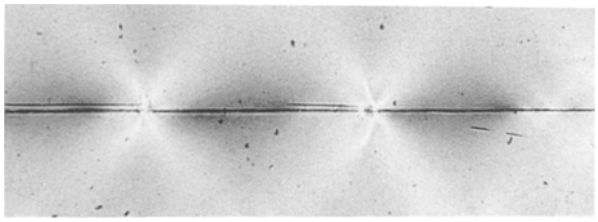

Figure 12 Stress birefringence pattern in Kevlar 149/epoxy monolayer demonstrating the occurrence of fragmentation in the Kevlar 149 para-aramid fibre.

filaments is shown. The video recordings clearly reveal that at a given load level a wide damage zone suddenly appears, covering the full width of the fibre array, as seen in the first picture of the series. We believe that as soon as one fibre becomes flawed at some point, the high sensitivity of the Kevlar 149 fibres to any load change (due to the load released at the fibre site) creates instantaneous damage (most probably splitting) in the neighbouring fibres, due, as we noted before, to the high flaw density in this fibre. From the sequence of pictures it is seen that the entire cross-section is progressively destroyed as a whole, and other similar damage zones suddenly appear as well. Clearly this mode of failure, and its dynamics, differ significantly from those of Kevlar 29/epoxy microcomposites, in which a progressive sequence of debonding occurs and a k^* (or its equivalent) is observed, and from that of Kevlar 49/epoxy microcomposites in which a progressive sequence of filament breaks is observed (but the validity of the k^* approach is not clear). This will be discussed further in the next section. In this case the typical statistical models for composite failure (see Appendix) are inadequate, because there is no sequence of fibre breaks leading to composite failure.

Fibre splitting is much more extensive in Kevlar 149 aramid fibres than in the other types of Kevlar fibres (compare Fig. 10 with Fig. 14), and is probably caused by the large density of flaws existing in the fibre, as shown elsewhere [50].

4.2.4. Kevlar 29/Kevlar 149/epoxy hybrid microcomposites

Four hybrid microcomposites with a configuration of $[K29/K149_2/K29]_s$ were tested. In Figs 15a to c, Young's modulus and the strength and failure strain are plotted against fibre content. In view of the small number of samples tested, no definite conclusions can be drawn, but as a whole the observations are similar to the previous cases. The photoelastic stress pattern observed during a quasistatic tensile test (Fig. 16) is a combination of the patterns seen previously in Kevlar 149/epoxy composites and in Kevlar 29/epoxy composites.

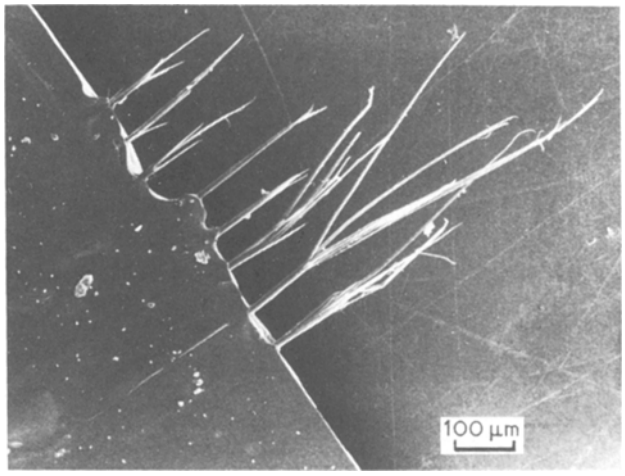

Figure 14 Scanning electron micrograph of a Kevlar 149/epoxy microcomposite monolayer after a fracture test.

4.2.5. E-glass/epoxy microcomposites

Four microcomposites containing one E-glass fibre and four microcomposites containing eight fibres were tested. Comparing the failure strains of E-glass and epoxy (Table I), there is a fair *a priori* probability that (random) fibre breakage will be the triggering fracture event in this system. In Figs 17a to c, Young's modulus, the strength and failure strain are plotted against the fibre volume fraction, respectively. The experimental data lie below the ROM line, but follow a line approximately parallel to the ROM in the case of modulus, strength, and possibly strain.

In a microcomposite containing one glass fibre, we have observed that straight and inclined conical cracks initiated at a fibre break and propagated throughout the matrix. Here, sufficient energy is released to propagate a crack in the matrix, producing complete failure of the specimen. This has been termed "high energy fracture" by other authors [43].

Fig. 18 shows the damage growth process in a microcomposite monolayer containing eight filaments. It can be seen that filaments break randomly at several sites. From the series of pictures shown in the figure, and from the video recordings, it is observed that successive fibre failure events occur in a given cross-section of the fibre array, and as soon as four adjacent failures occur ($k^* = 4$), fast failure suddenly occurs. This case is the closest to the process assumed in statistical theories of failure (see Appendix). SEM and optical microscope photographs of fractured glass/epoxy microcomposite monolayers revealed very short pull-out lengths for glass ($\approx 25\,\mu m$). Fig. 4 is a scanning electron micrograph of an E-glass/epoxy monolayer fractured cross-section. The high quality of this particular monolayer is revealed by the constant interfibre distance and the very thin monolayer obtained. Fig. 19 is an optical microscope view of an E-glass/epoxy monolayer after fracture which shows typical debonded zones, of length about three fibre diameters.

Figure 13 Damage growth in Kevlar 149/epoxy microcomposite monolayer: (a) a fast failure event occurs within the whole fibre array cross-section in a given site at RS = 0.985; (b) a second, independent, failure event occurs at RS = 0.992 in a mode similar to the first event; (c) and (d) damage grows in intensity as seen from birefringent pattern and the zone inbetween the two sites involved is progressively unloaded (colour turns darker); (e) final break at RS = 0.925.

4.2.6. Pull-out length considerations

A simple relationship exists between the (average) critical transfer length l_c of a fibre, its (average) strength σ_f, and the interface strength (or, more correctly, the shear transfer ability of the interface [49]) τ, namely

$$\tau = \frac{\sigma_f d_f}{2l_c} \quad (2)$$

where d_f is the fibre diameter. Using microcomposite monolayers as in the present work, the stress in a fibre at which a break appears can be retrieved from the value of the applied stress, and the pull-out length can be measured, because out experimental apparatus permits overall viewing of the failure process. Assuming that the pull-out length and the critical length of the fibre are formally related, one can, in principle, evaluate the shear transfer ability of the interface using Equation 2. This was not performed here, however, because in several cases the fracture process was complicated by parasite fracture events caused by the rough edges of the samples, voids, etc., and only a few samples were tested. A systematic study of this will be performed in the near future.

4.3. Dynamics of the failure process

In Kevlar 29/epoxy microcomposite monolayers, a succession of debondings and matrix cracks culminates in fast failure after the fourth fibre is reached. Whether or not failure proceeds from a side crack, it appears that fibre–fibre interactions do play a role in this system. In Kevlar 49 microcomposites, once the first filament breaks (or splits) at a weak site, a matrix crack develops at this site laterally, and a slow sequence of filament failures and matrix cracking is observed without ever reaching the state of catastrophic failure. In other words in this system there is no k^*, or else k^* is larger than 8. Little fibre–fibre correlation seem to exist in this microcomposite system, or if it does it is in a much weaker form than in the Kevlar 29 composite perhaps due to differences in geometry between the systems. In Kevlar 149 microcomposites, after the appearance of the first filament failure at a weaker site and transmission of the overload on the adjacent fibres, all adjacent fibres in the array show almost instantaneously some damage which increases rapidly in intensity until the matrix starts to fail, this peculiar damage mode occurring simultaneously at other sites as well. Thus strong fibre–fibre correlations exist in this system. By contrast, in E-glass microcomposites a slow sequence of adjacent filament failures is observed, but in this case without any matrix crack propagation between the fibres, and k^* is about 4. Fibre–fibre correlations in this system are weak but do exist because failure occurs in a single (critical) cross-section.

The differences in failure modes and dynamics may be explained in several ways, based on the preliminary results presented here. The edge-to-edge interfibre distance of the Kevlar 49 and E-glass microcomposite (65 μm, thus approximately 4.5 times the diameter of the glass fibre and 5.5 times that of the Kevlar 49 fibre), is larger than the interfibre distance in the Kevlar 149 microcomposites (40 μm, approximately three times the diameter of the fibre). This represents almost a limit case, because when the interfibre distance is more than five to six fibre diameters, there is almost no interaction between the fibres [36, 43]. In view of this, once a first fibre break occurs in E-glass and Kevlar 49 composites, there is less overload in adjacent filaments than in Kevlar 149 composites. Therefore, failure of the neighbouring filaments will

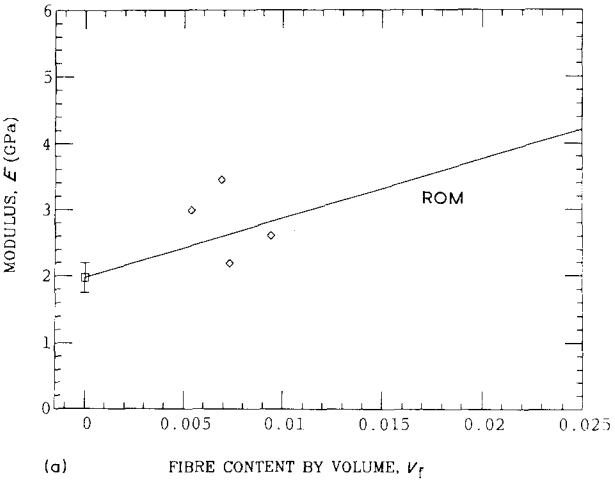

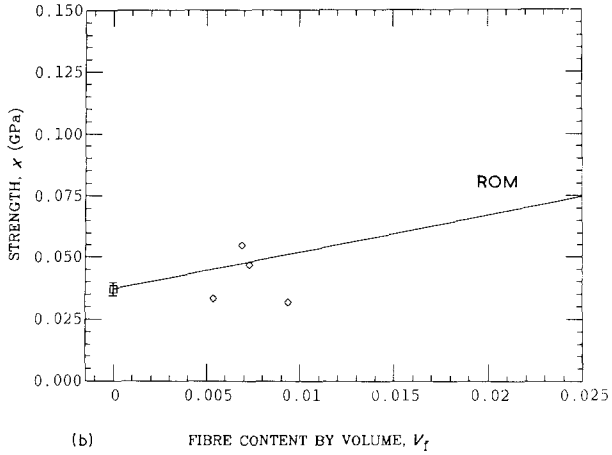

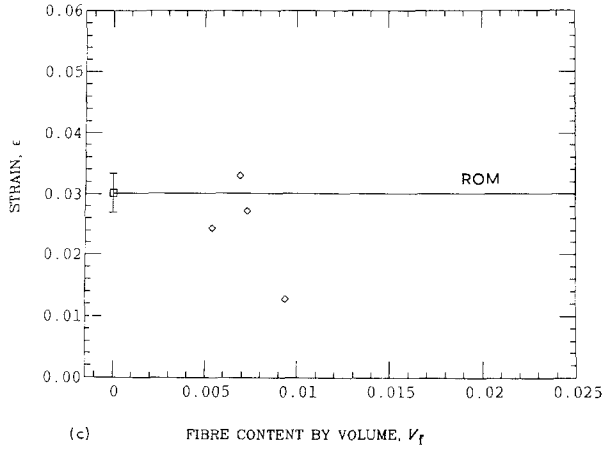

Figure 15 (a) Young's modulus, (b) tensile strength, (c) tensile strain at failure as a function of fibre content in hybrid Kevlar 29/Kevlar 149/epoxy microcomposite monolayers (K29/K149/CY223–HY956). (□) Epoxy film (95% c.i.), (◇) eight-fibre monolayers.

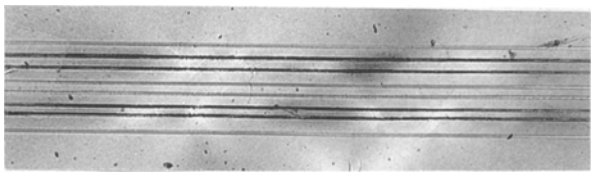

Figure 16 Stress birefringence pattern in hybrid Kevlar 29/Kevlar 149/epoxy monolayer with a $[K29/K149_2/K29]_S$ configuration.

take place at a higher overall stress and, consequently, the crack propagation speed is lower in E-glass and Kevlar 49 composites. Regarding the mode of failure, in the case of the Kevlar 49 composite there seems to be no direct effect of the first filament break on the neighbouring filaments (the neighbouring filaments break because of matrix crack propagation), whereas in the E-glass case the effect is very pronounced. One reason for this may be again based on the difference in interfibre distance between these two systems, and also on the fact that because glass is very brittle, once a weak point fails the break is total, whereas in the aramid fibre the break may start as a partial split which grows slowly and longitudinally along the fibre, thereby retarding the process of load transmission towards the adjacent fibres. In Kevlar 149 microcomposite monolayers, both the smaller interfibre distance and the relatively high sensitivity of the fibre to applied loads in adjacent fibres (due to the high density of defects) have a strong influence on both the dynamics and the mode of failure of this system. When the first filament fails (which occurs at relatively high loads because of the high strength of this fibre), the probability of finding a critical flaw in the neighbouring fibres in the same segment of the composite is much larger for Kevlar 149 than for E-glass or Kevlar 49, and so the probability of inducing a break in a neighbouring fibre is large. This could explain the high speed of the damage propagation across the entire width of the monolayer as well as the failure mode. Note that the occurrence of such a failure process makes it impossible, apparently, for the fibre fragmentation process to take place as it does in a single Kevlar 149 fibre microcomposite.

Perhaps another way to explain differences in failure dynamics is by taking the difference in fibre shape parameters (8.7 for Kevlar 149 and 4.8 for E-glass) into account. The higher the shape parameter, the lower the variability and thus the more uniform the strength is, and the higher the probability that neighbouring filaments fail in the same cross-section because of overload after the first filament failure. Thus high speed of failure propagation will occur, all other parameters being equal. If the shape parameter is low, the probability of finding a much stronger element in the neighbouring fibres is higher, and a lower propagation speed is expected.

To summarize our observations regarding the mode of failure in each system, keeping in mind that differences in geometry exist between the various cases, the E-glass/epoxy monolayer is the case which can be best described by current stochastic models (see the Appendix); the Kevlar 29/epoxy monolayer may perhaps also be described by such stochastic model at the condition that a zone of fibre failure (as long as the debonding/splitting length), rather than a fibre snapping "point", is considered; the Kevlar 49/epoxy monolayer containing eight fibres, at the interfibre distance considered here, is either not well described by the statistical model, or is out of the range of its application due to too large an interfibre distance, but it is also possible that the critical cluster is larger than eight fibres; finally, the statistical model currently utilized for the description of the failure mode of fibre-dominated composites is clearly not valid in the case of Kevlar 149/epoxy monolayers.

A qualitative model for the failure process in Kevlar 149/epoxy may be outlined as follows. Because fibre failure in individual fibres proceeds by a splitting/fibrillation mechanism, it can be assumed that at a given applied stress part of the load only, rather than its entirety, is redistributed from a split site on to the nearest neighbours. But because the Kevlar 149 fibre has a large defect density, it is extremely sensitive to any local load increase. Therefore the nearest neighbours start failing immediately by splitting and this itself is transmitted almost instantaneously to the next nearest neighbours and so on. A relatively wide damage zone (along the fibre length) is involved because splitting takes place in a "delocalized" way as explained earlier. Such damage zone growth process does not appear in other aramid monolayer systems because the flaw density is much lower in these fibres.

Only a limited number of samples was tested in this preliminary study, thus it is difficult to assess the validity of such explanations. More work with each individual microcomposite monolayer system is obviously needed before definitive conclusions are reached.

5. Conclusions

A new experimental approach was proposed for the study of damage and failure in model unidirectional composite materials containing carefully positioned single fibres of various types. A special fabrication technique for the manufacturing of such microcomposite monolayers was developed and a limited number of samples of several types were mechanically tested using a specially designed microtensile testing apparatus. The damage nucleation and growth process was followed by video microphotography. This approach is considered to be potentially important for accurate studies of the effects of the following variables on the micromechanics and modes of failure in composite materials: chemical modification of the fibre/matrix interfacial layer, matrix modification, fibre–fibre interactions (fibre bunching), fibre misalignment or slack, fibre configuration in hybrid composites, failure dynamics (crack speed variations), and more. In addition, and most importantly, our approach may yield key information on the assessment of various materials parameters (such as the critical crack size, k^*, or the correlation length δ), it may serve as a tool in the validation of theoretical models for failure such as the statistical/probabilistic schemes or the Rule-of-

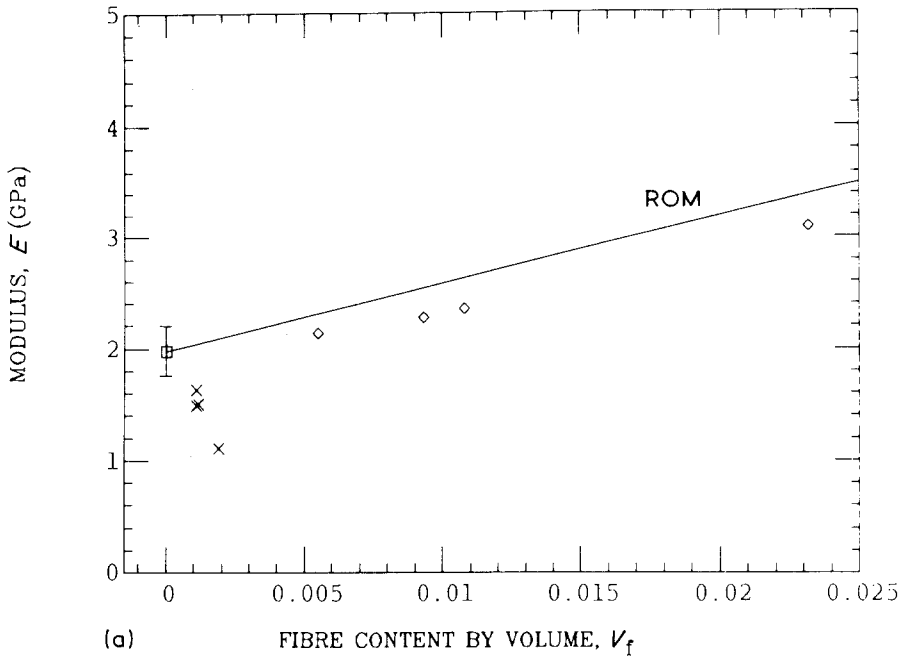

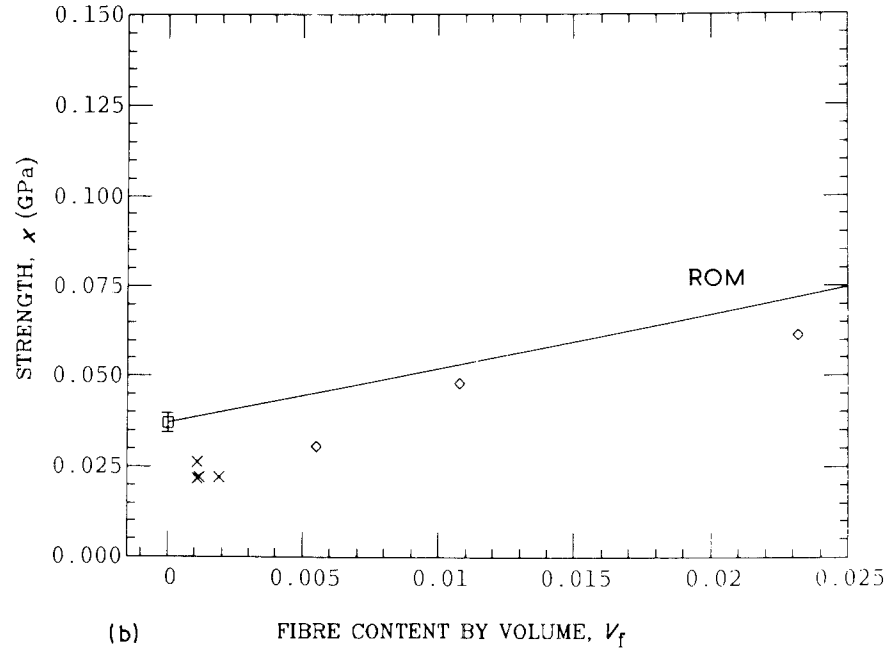

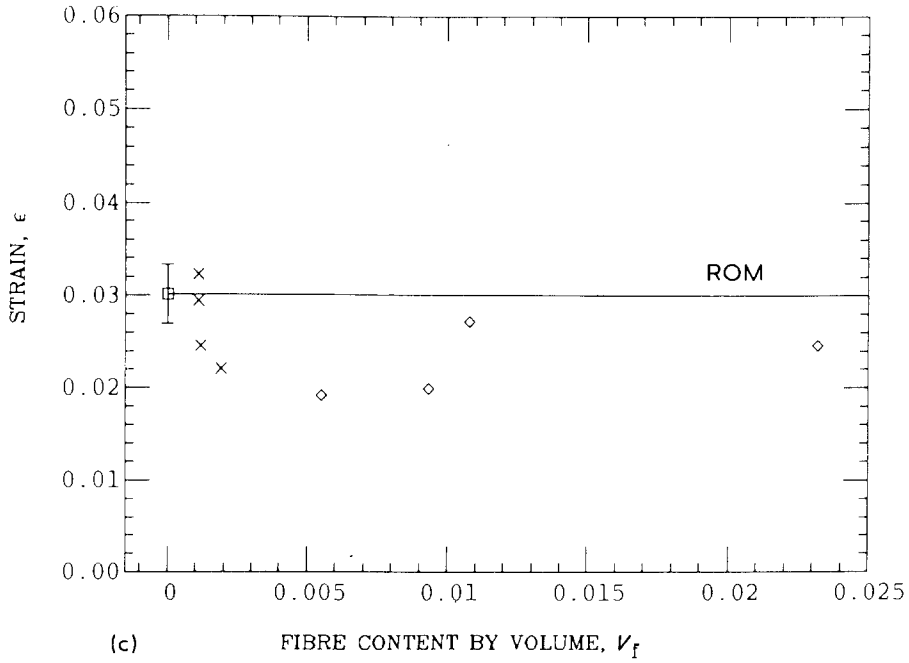

Figure 17 (a) Young's modulus, (b) tensile strength, (c) tensile strain at failure as a function of fibre content in E-glass/epoxy microcomposite monolayers (E-glass/CY223–HY956). (□) Epoxy film (95% c.i.), (x) one-fibre monolayer, (◇) eight-fibre monolayer.

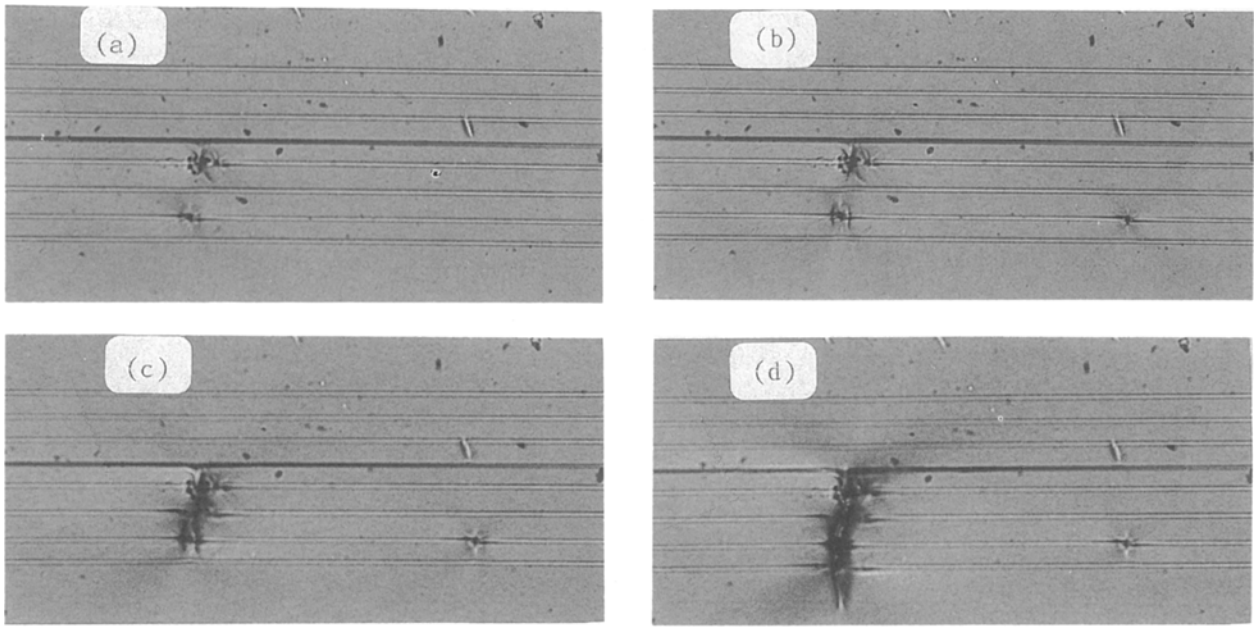

Figure 18 Damage growth in E-glass/epoxy microcomposite monolayer: (a) RS = 0.90, two breaks are seen in fibre 5 and fibre 7 (from top); (b) stress increase up to RS = 0.94, an additional, independent, break occurs in fibre 7; (c) RS = 1.00, a cluster of $k = 3$ is formed in fibres 5, 6 and 7; (d) RS = 1.00, the cluster grows very rapidly to $k = 4$ and fast final failure occurs (thus $k^* = 3$ or 4).

Mixtures scheme, and it may throw some light upon the occurrence of new modes of failure.

We consider the major conclusions of the present research to be as follows.

1. The fabrication technique of the microcomposite monolayers is extremely reliable and relatively simple: accurate interfibre distances are obtained and the fibres lie in a plane. In the case of thicker ($> 40\,\mu$m) films, however, this plane lies closer to one face, and future work will focus on refining the technique to obtain thinner monolayers, both to avoid this fibre plane positioning problem and to obtain microcomposites possessing higher fibre volume fraction. Regarding this last point, the fibre volume fraction was limited here to about 0.02. This has now been increased in our laboratory by more than one order of magnitude in a limited number of new samples for future studies by (i) reducing the monolayer thickness, (ii) reducing the interfibre distance, and (iii) by using a new adjustable die which can, in principle, be used to cut samples with a much smaller width.

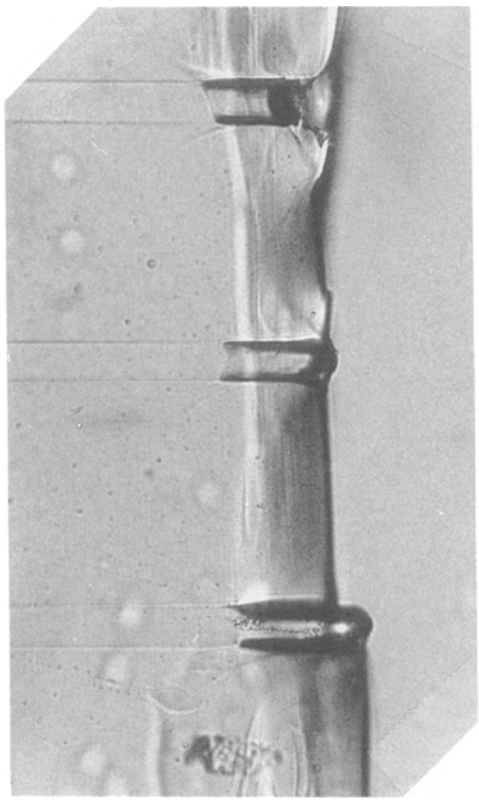

Figure 19 Optical microscope view of a failed E-glass/epoxy monolayer showing debonded zones about 2 to 3 fibre diameters long.

2. A definite correlation exists between both Young's modulus and the tensile strength of all microcomposite monolayers and the fibre volume fraction. This correlation is much weaker, in general, for the failure strain. For all types of microcomposite monolayers, Young's modulus follows quite accurately the Halpin–Tsai equation (the Rule-of-Mixture), even at the very low volume fractions of fibres used. These results are encouraging because they confirm that the manufacturing technique developed yields microcomposite monolayers of good quality.

3. The failure mode and failure dynamics of the microcomposites vary from system to system. This may be due to differences in interfibre distance among the various systems, differences in the shape parameter of fibres, and differences in the density of flaws along the length of the fibre. E-glass/epoxy microcomposite monolayers fail by a cascade of successive fibre breaks, and beyond four adjacent fibre breaks failure proceeds in a catastrophic way. This case is well described by current probabilistic schemes. Kevlar 29/epoxy microcomposite monolayers fail by a cascade of fibre/matrix debonding events and again,

as soon as four such adjacent events occur, failure is catastrophic. The validity of the existing probabilistic schemes is in doubt here, although the concept of a critical crack "zone" could be valid. Kevlar 49/epoxy microcomposite monolayers fail by a progressive cascade of fibre breaks, much like in the case of E-glass composites, but no critical point is ever observed in this system. Finally, Kevlar 149/epoxy microcomposite monolayers behave in a very different way compared to the previous systems, because a fast propagating wide damage zone is observed to nucleate and grow across the entire width of the fibre array, as soon as damage nucleates at a weak point in a fibre. This process occurs simultaneously at various locations along the sample length. Current theoretical schemes apparently do not deal with such failure mode.

Acknowledgements

This work was supported by a grant from the National Council for Research and Development, Israel, and the K.F.A. Juelich, Germany. The authors thank Mr A. Waterink, and the Graphics and Design and the Mechanical Workshop Departments, Weizmann Institute, for their professional help with some of the experimental aspects of this work. Dr Ron Gulino, Professor S. Leigh Phoenix and Professor Peter Schwartz, Cornell University, are thanked for stimulating conversations and advice.

Appendix

To gain some insight into the physics of the failure of unidirectional composites, an approximate theoretical model for the failure of microcomposite monolayers is presented (see also Smith [53, 54]). The main objective of this simple calculation is to identify the fundamental characteristics and key parameters involved in the failure process of microcomposite monolayers, that is those parameters which should be focused upon in experiments. Several simplifying assumptions will be made which, however, do not necessarily correspond exactly to the experimental reality.

1. A Weibull distribution is assumed to represent satisfactorily the strength distribution of single fibres.
2. A state of pure tension exists in the fibres, and the matrix transfers stress to these only by a shearing mechanism.
3. The fibres are perfectly linear elastic materials which fail in a brittle mode ("snapping").
4. The interfacial zone is considered to have infinite strength and thus no fibre/matrix debonding exists.

A short segment of a microcomposite monolayer of length δ containing N fibres, is assumed (refer to Fig. 1). For small stress x (per fibre) the probability of at least one fibre failure in the bundle is approximately N times the probability of a single fibre failure. Assuming that the fibre strength follows the Weibull distribution, Equation 1, this is approximately equal to

$$N\delta\left(\frac{x}{a}\right)^b$$

for $x \ll a$ (small stress relative to the mean strength of the sample), and for relatively small values of the coefficient of variation. As b ranges typically from 4 to 20 this last assumption is justified in most cases. Given one failure in a fibre, the probability that at least one of its two nearest neighbours fails under the enhanced stress $K_1 x$, where K_1 is a stress enhancement factor, is then

$$\approx 2\delta\left(\frac{K_1 x}{a}\right)^b$$

Hence the probability that there is at least one pair of adjacent fibre failures is found by multiplying the previous two expressions, thus

$$\approx 2N\delta^2\left(\frac{x}{a}\right)^b\left(\frac{K_1 x}{a}\right)^b$$

This progressive failure process continues: given two adjacent failures, the probability that at least one of their two adjacent neighbours fails is

$$\approx 2\delta\left(\frac{K_2 x}{a}\right)^b$$

where K_2 is the stress enhancement factor due to the release of the load from two adjacent fibre breaks, and so on. The probability that there is at least one group of k adjacent failures (a k-plet, using the terminology of Batdorf [55]), for small k and x, is

$$\approx 2^{k-1}N\delta^k\left(\frac{x}{a}\right)^b\prod_{i=1}^{k-1}\left(\frac{K_i x}{a}\right)^b$$

As soon as k reaches a critical value k^*, which depends on the material system, the stress concentrations become so large that further fibre failures are almost certain. This defines the probability of failure of the segment of microcomposite monolayer of length δ under a stress x, $F_\delta(x)$, which is the same as the probability of occurrence of a critical group of k^* adjacent failures given above. Thus, with some rearrangement

$$F_\delta(x) \approx 2^{k^*-1}N\delta^{k^*}(K_1 K_2 \ldots K_{k^*-1})^b\left(\frac{x}{a}\right)^{k^*b} \quad \text{(A1)}$$

which is identical to a result derived by Smith in a different way (see Equation 4.3, with $\delta = 1$, in Smith [54]). By rewriting Equation A1, one has therefore for the monolayer segment of length δ

$$F_\delta(x) \approx \left(\frac{x}{\alpha_\delta}\right)^\beta \quad \text{(A2)}$$

where

$$\beta = k^*b \quad \text{(A3)}$$

and

$$\alpha_\delta = a2^{(1-k^*)/k^*b}N^{-1/k^*b}\delta^{-1/b}(K_1 K_2 \ldots K_{k^*-1})^{-1/k^*} \quad \text{(A4)}$$

Now, the weakest-link rule gives the probability of failure $F_L(x)$, under a stress x, of a chain-like structure of length L made up of smaller segments of length δ, in terms of $F_\delta(x)$, as follows

$$F_L(x) = 1 - \{1 - F_\delta(x)^L\} \quad \text{(A5)}$$

that is

$$F_L(x) \approx LF_\delta(x) \quad (x \ll \alpha_\delta) \quad \text{(A6)}$$

By combining Equations A2 and A6, we obtain an approximate result for the probability of failure of a microcomposite monolayer of length L

$$F_L(x) \approx \left(\frac{x}{\alpha_L}\right)^{\beta} \quad \text{(A7)}$$

where α_L is given by Equation A4 multiplied by $L^{-1/\beta}$. If Equation A7 is viewed as the first term of a MacLaurin series, the probability of failure of the microcomposite monolayer of length L takes the final form

$$F_L(x, N) \approx 1 - \exp\left[-\left(\frac{x}{\alpha_L}\right)^{\beta}\right] \quad \text{(A8)}$$

which has the Weibull form. If we compare these approximations with Weibull's early model, applicable to a single-fibre element, it is seen that the concept of single critical defect in a fibre is replaced by that of a critical group of k^* defects adjacent to each other. The Weibull form is thus obtained for a fibrous assembly, with shape and scale parameters given as functions of the parameters of the parent (single fibre) Weibull distribution and of other material parameters, through Equations A3 and A4. Batdorf [55] proposed a similar approximate model from a slightly different viewpoint, and Smith [54] and Manders *et al.* [56] have produced Monte Carlo simulations on the same problem.

From the simple model just presented, is follows that the key parameters to aim at from the experimental viewpoint are k^*, a, b, δ, and the K_i. Once this is done, the probability of failure of the microcomposite monolayer is completely determined, and the validity of the assumptions in the theoretical model may be assessed.

References

1. H. D. WAGNER, in "Application of Fracture Mechanics to Composite Materials", edited by R. B. Pipes and K. Friedrich (Elsevier Science, 1988) pp. 39–77.
2. L. W. STEENBAKKERS and H. D. WAGNER, Polymeric Composites Laboratory, Materials Research Department, The Weizmann Institute of Science Report PCL-88-02 (1988).
3. S. L. PHOENIX, P. SCHWARTZ and H. H. ROBINSON IV, *Compos. Sci. Technol.* **32** (1988) 81.
4. H. E. DANIELS, *Proc. Roy. Soc. Lond.* **A183**, (1945) 404.
5. B. D. COLEMAN, *J. Mech. Phys. Solids* **7** (1959) 66.
6. D. E. GUCER and J. GURLAND, *ibid.* **10** (1962) 365.
7. P. M. SCOP and A. S. ARGON, *J. Compes. Mater.* **1** (1967) 92.
8. B. W. ROSEN, *AIAA J.* **2** (1964) 1985.
9. C. ZWEBEN, *ibid.* **6** (1968) 2325.
10. P. M. SCOP and A. S. ARGON, *J. Compos Mater.* **3** (1969) 30.
11. C. ZWEBEN and B. W. ROSEN, *J. Mech. Phys. Solids* **18** (1970) 189.
12. A. S. ARGON, in "Composite Materials", Vol. 5, edited by L. J. Broutman (Academic, New York, 1974) pp. 154–90.
13. R. L. SMITH, S. L. PHOENIX, M. GREENFIELD, R. B. HENSTENBURG and R. E. PITT, *Proc. Roy. Soc. Lond.* **A388** (1983) 353.
14. W. WEIBULL, *Handlingar (Royal Swedish Academy of Energy Sciences)* **151** (1951).
15. H. D. WAGNER, S. L. PHOENIX and P. SCHWARTZ, *J. Compos. Mater.* **18** (1984) 312.
16. H. D. WAGNER, P. SCHWARTZ and S. L. PHOENIX, *J. Mater. Sci.* **21** (1986) 1868.
17. J. GUTANS and V. TAMUZS, *Mech. Compos. Mater.* **20(6)** (1984) 1107 (in Russian).
18. A. S. WATSON and R. L. SMITH, *J. Mater. Sci.* **20** (1985) 3260.
19. H. D. WAGNER, (1988) *J. Macromol. Sci.-Phys.* (1989) in press.
20. P. RAY and B. K. CHAKRABARTI, *J. Phys. C Solid State Phys.* **18** (1985) L185.
21. *Idem, Solid State Commun.* **53(5)** (1985) 477.
22. S. L. PHOENIX and L.-J. TIERNEY, *Eng. Fract. Mech.* **18** (1983) 193.
23. C. C. KUO and S. L. PHOENIX, Sibley School of Mechanical and Aerospace Engineering, Cornell University, Ithaca, New York, Report MSD-83-02 (1983).
24. D. SORNETTE, *J. Phys. France* **49** (1988) 889.
25. S. L. PHOENIX, Proceedings 9th US National Congress of Applied Mechanics Book No. H0028, (The American Society of Mechanical Engineers, New York, 1982) p. 219.
26. J. M. HEDGEPETH, NASA TN D-882 (1961).
27. J. M. HEDGEPETH and P. VAN DYKE, *J. Compos. Mater.* **1** (1967) 294.
28. W. B. FICHTER, NASA TN D-5453 (1969).
29. D. G. HARLOW and S. L. PHOENIX, *J. Compos. Mater.* **12** (1978) 195.
30. *Idem, ibid.* **12** (1978) 314.
31. H. FUKUDA and K. KAWATA, *Fibre Sci. Technol.* **9** (1976) 189.203.
32. E. D. REEDY Jr, *J. Compos. Mater.* **18** (1984) 595.
33. S. B. BATDORF and R. W. C. KO, *AIAA J.* **23** (1985) 1749.
34. M. G. BADER and M. J. PITKETHLY, in "Mechanical Characterisation of Fibre Composite Materials, edited by R. Pyrz (Aalburg University, Denmark, 1986).
35. L. C. WOLSTENHOLME and R. L. SMITH, Technical Report No. 62, Department of Mathematics, University of Surrey, Guilford, (1988).
36. D. M. SCHUSTER and E. SCALA, *Trans. Met. Soc. AIME* **230** (1964) 1635.
37. W. R. TYSON and G. I. DAVIES, *Brit. J. Appl. Phys.* **16** (1965) 199.
38. D. PIH and D. R. SUTLIFF, AFML-TR-68-380 (1968).
39. T. F. MACLAUGHLIN, *J. Compos. Mater.* **2** (1968) 44.
40. R. B. McKEE Jr and G. SINES, *J. Elastoplastics* **1** (1969) 185.
41. E. FRIEDMAN, Proceedings of the 22nd Conference SPI Reinforced Plastics Division, Section 4-A (1967).
42. A. E. ARMENAKAS, S. K. GARG, C. A. SCIAMMARELLA and V. SVALBONAS, *Exp. Mech.* **12** (1972) 1.
43. J. MULLIN, J. M. BERRY and A. GATTI, *J. Compos. Mater.* **2** (1968) 82.
44. W. A. FRASER, F. H. ANCKER, A. T. DIBENEDETTO and B. ELBIRLI, *Polym. Compos.* **4(4)** (1983) 238.
45. L. T. DRZAL, M. J. RICH, M. F. KOENIG and P. F. LLOYD, *J. Adhes.* **16** (1983) 133.
46. D. JACQUES and J. P. FAVRE, Proceedings of the 6th International Conference on Composite Materials (ICCM-6) and 2nd European Conference Composite Materials (ECCM-2) Vol. 5, edited by F. L. Matthews, N. C. R. Buskell, J. M. Hodgkinson, J. Merton, 20-24 July 1987, (Elsevier Applied Science, London, 1987) pp. 471–80.
47. W. D. BASCOM, R. M. JENSEN and L. W. CORDNER, *ibid.* pp. 424–38.
48. M. R. PIGGOTT, A. SANADI, P. S. CHUA, D. ANDISON, in "Composite Interfaces" edited by H. Ishida and J. L. Koenig (North-Holland, New York, 1986) p. 109.
49. L. DiLANDRO, A. T. DIBENEDETTO and J. GROEGER, *Polym. Compos.* **9(3)** (1988) 209.
50. L. W. STEENBAKKERS and H. D. WAGNER, *J. Mater. Sci. Lett.* **7** (1988) 1209.
51. A. S. TAYLOR and H. D. WAGNER, (1989) submitted.
52. P. G. RIEWALD, A. K. DHINGRA, T. S. CHERN, Proceedings of the 6th International Conference on Composite Materials (ICMM-6) and 2nd European Conference on Composite Materials (ECCM-2), Vol. 5, edited by F. L.

Matthews, N. C. R. Buskell, J. M. Hodgkinson, J. Merton, 20–24 July 1987 (Elsevier Applied Science, London, 1987) pp. 362–70.
53. R. L. SMITH, Paper presented to the IUTAM Symposium on Probabilistic Methods in the Mechanics of Solids and Structures, Stockholm, Sweden, June 19–21 (1984).
54. R. L. SMITH, *Proc. Roy. Soc. Lond.* **A372** (1980) 539.
55. S. B. BATDORF, *J. Reinf. Plast. Compos.* **1** (1982) 153.
56. P. W. MANDERS, M. G. BADER and T.-W. CHOU, *Fibre Sci. Technol.* **17** (1982) 183.

Received 14 October
and accepted 14 November 1988

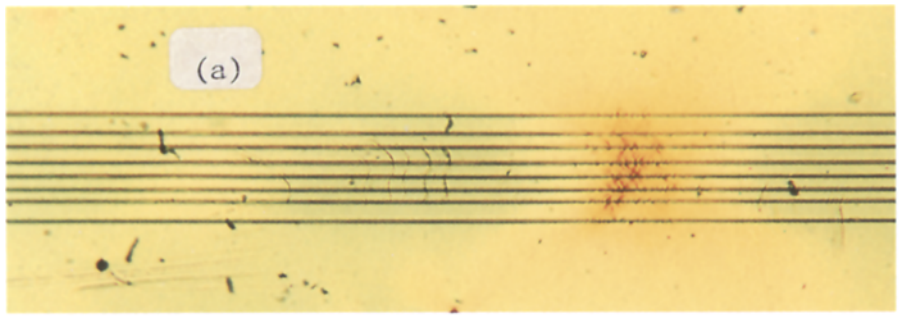
(a)

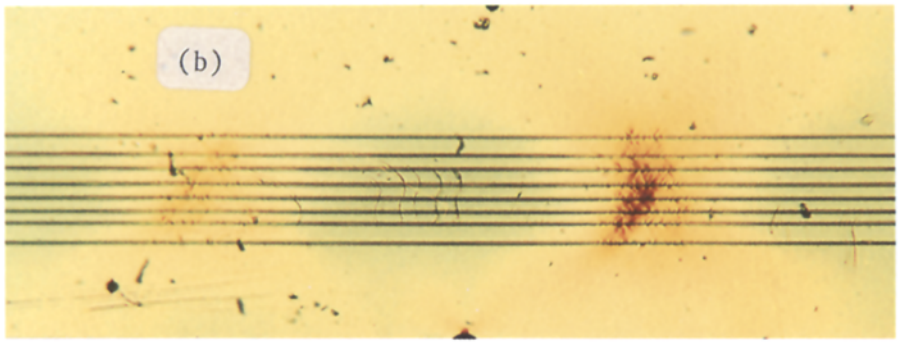
(b)

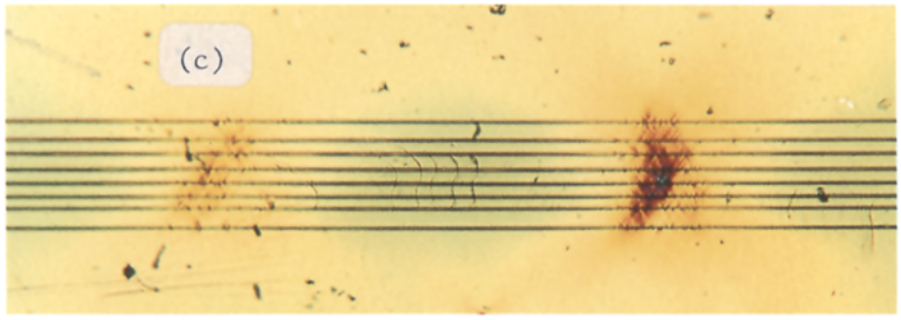
(c)

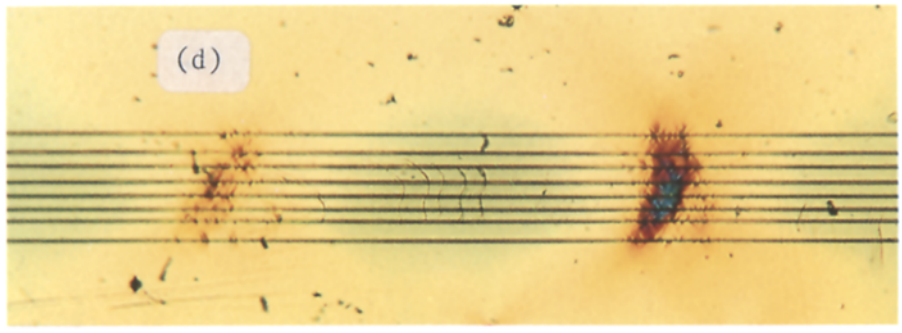
(d)

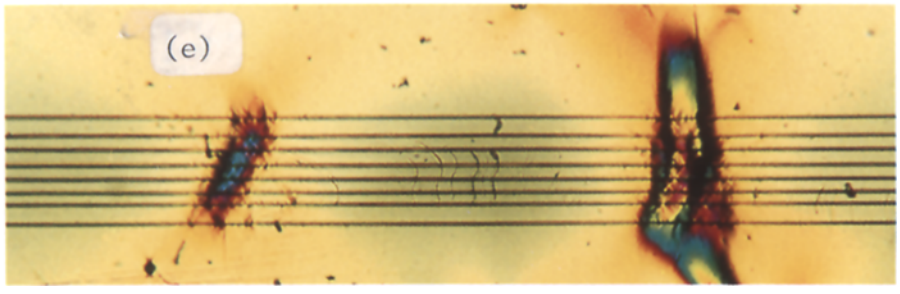
(e)